HY
HJ-1AB
CBERS
Gaofen
Beijing-2
Sentinel-1
Sentinel-2
Sentinel-3
Sentinel-5p
Aeolus

2023 DRAGON 5 SYMPOSIUM

3rd YEAR RESULTS REPORTING

11-15 SEPTEMBER 2023

Synergistic Monitoring of Sea Ice from Multi-sensors

(ID: 57889)

Xi Zhang, Wolfgang Dierking, Li-jian Shi, Marko Mäkynen
Juha Karvonen, Rasmus Tonboe, Xiao-yi Shen, Mei-jie Liu

Outline

I. Introduction
II. Main results
III. Cooperation
IV. Young scientists and Publications
V. Next planning

I. Introduction

Objective

Upgrade and develop methodologies to retrieve quantitative sea ice information including measurements of thickness, drift, concentration, and detection of icebergs.

- Satellite data: Sentinels, ALOS-1/2, SMOS, CryoSAT-2, CFOSAT; HY-2, GF series
- Arctic, Antarctic and regional sites with seasonal ice cover

Dragon-2 5290	Dragon-3 10501	Dragon-4 32292, Part I	Dragon-5 57889
Only SAR Types	SAR + Optical Types, thickness, drift	Altimeter + SAR Thickness, deformation/drift	Multiple data More ice parameters

Team Composition

European Partners

- Prof. Dr. Wolfgang Dierking (PI) — University in Tromsø, Norway; Alfred Wegener Institute Helmholtz Center for Polar and Marine Research, Germany.
- Dr. Marko Mäkynen and Dr. Juha Karvonen — Finnish Meteorological Institute, Finland
- Dr. Rasmus Tonboe — Technical University of Denmark, Denmark

Chinese Partners

- Dr. Xi Zhang (PI) — First Institute of Oceanography, Ministry of Natural Resources
- Dr. Li-jian Shi, Tao Zeng and Qian Feng — National Satellite Ocean Application Service
- Dr. Jie Liu and Zhi Yuan — Institute of Spacecraft System Engineering, China Academy of Space Technology
- Dr. Xiao-yi Shen — Nanjing University
- Dr. Zhen-yu Liu — South-Central Minzu University
- Dr. Mei-jie Liu — Qingdao University

II. Main Results

1. Sea ice classification with multi-frequency SAR data during freezing and melting period
2. Sea ice surface and bottom morphology observation with SAR data
3. Sea ice drift detection with FY-3D microwave radiometer data
4. Snow depth retrieval over sea ice using microwave radiometer data
5. Analysis of decadal changes of ice in the Bohai Sea with GOCI data

1. Sea ice classification during melting period with SAR data

Objective

- Current studies primarily focus on SAR sea ice classification during the freezing-up period
- Surface meltwater can affect the identification of sea ice types.
- The use of SAR for type identification during melting ice may be a problem.

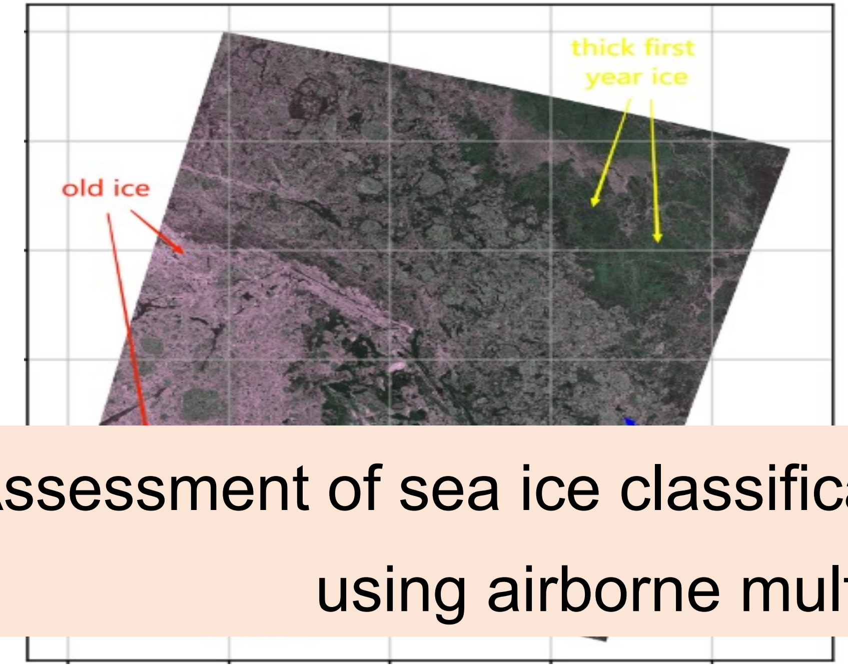

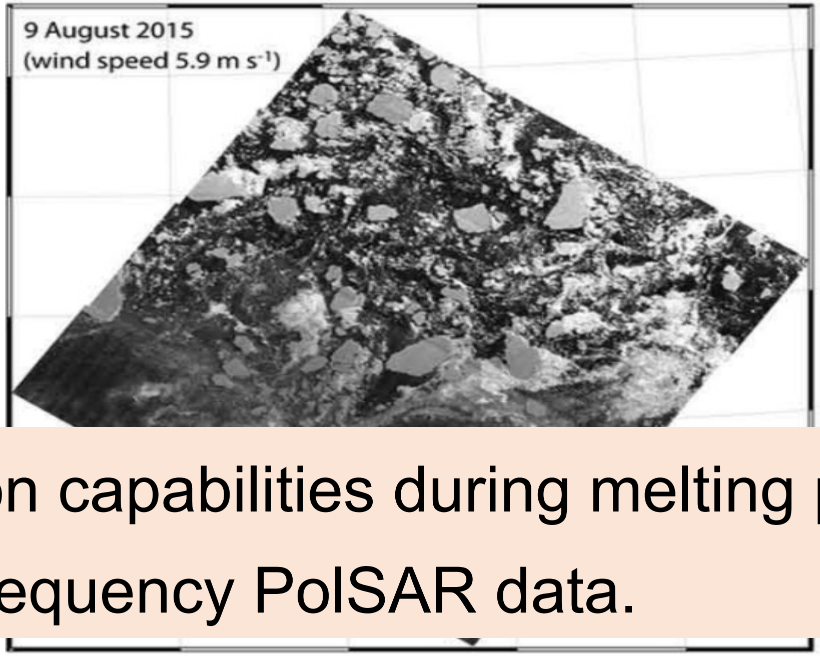

Assessment of sea ice classification capabilities during melting period using airborne multi-frequency PolSAR data.

Airborne Multi-frequency PolSAR data

- Time(UTC): 2022-02-27 06:22:54
- Frequency: L/S/C
- Resoultion: 1/1/0.5 m
- Flight altitude： 4710 m
- Incidence angle: 31°~34°
- Temperatures: 6~10℃
- Wind speed: 3~8 m/s

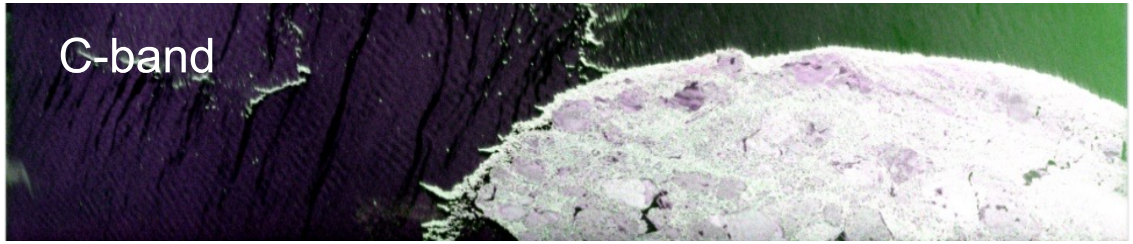

Sentinel-2 MSI data

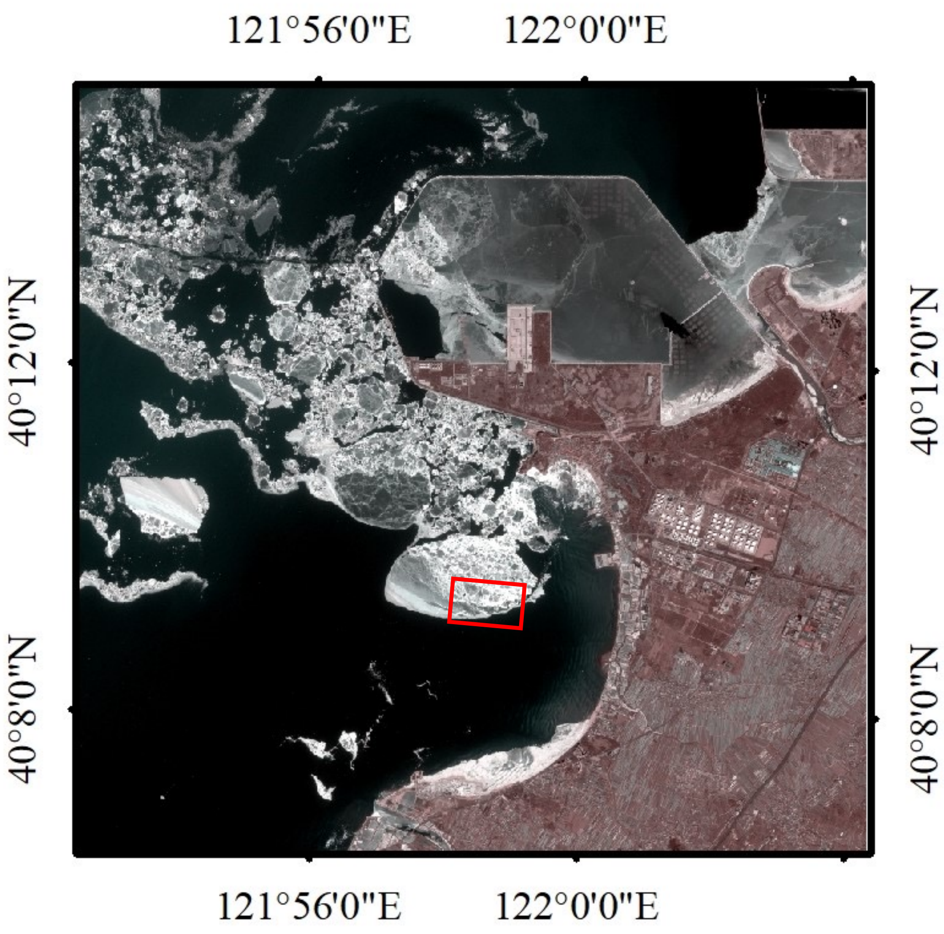

UC Time: 2022-02-27 02:36:39

4-hour ahead of SAR data

Visual interpretation

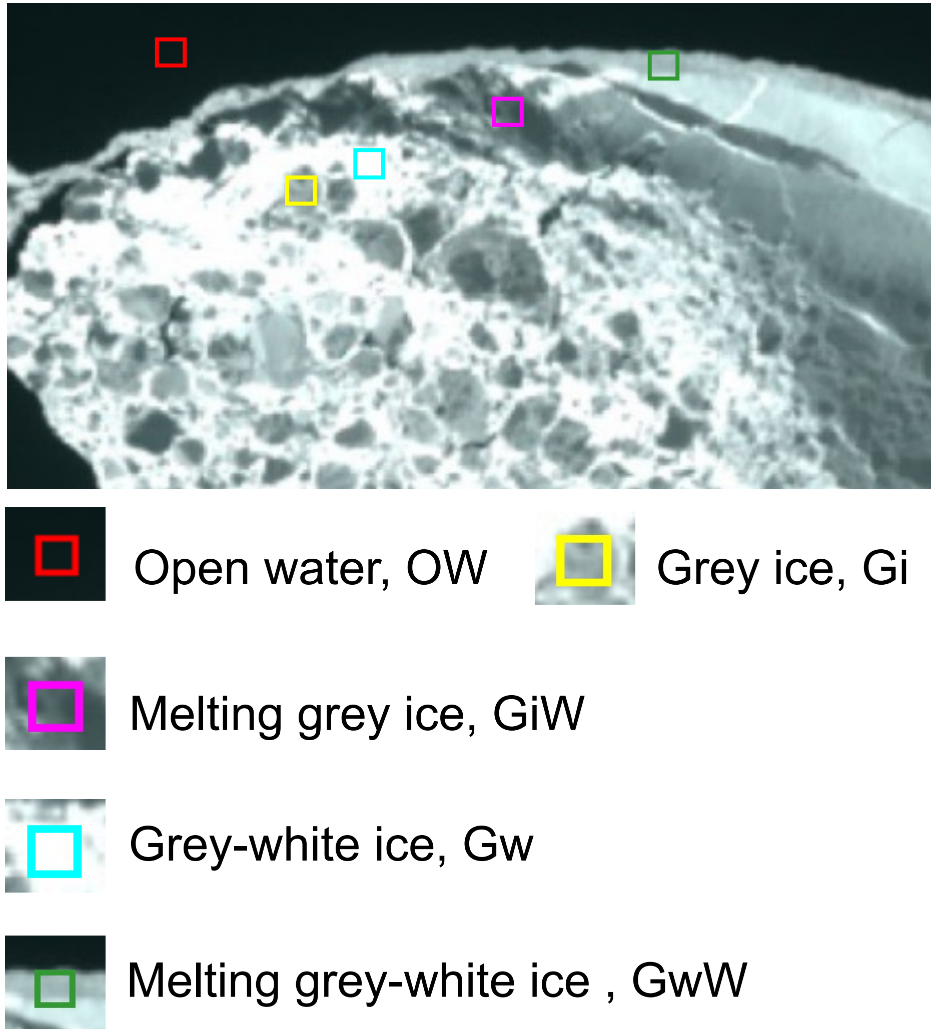

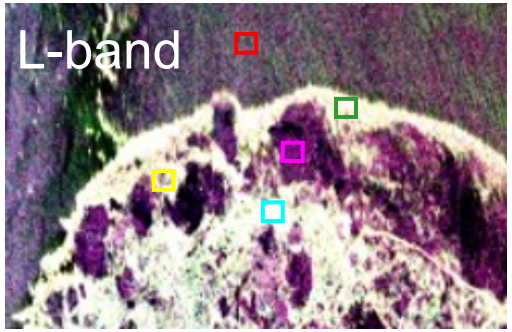

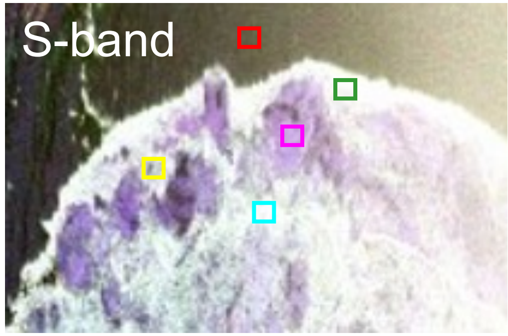

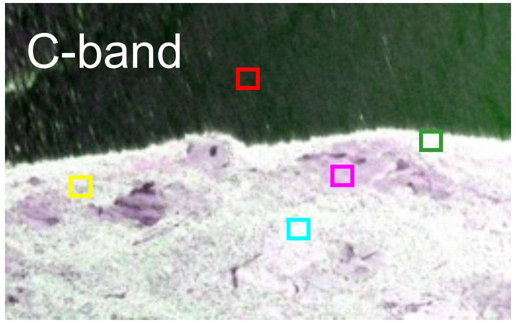

Method

The sea ice type discrimination ability of 51 polarization features in 3 bands was evaluated

The target polarization decomposition based scattering model	Freeman-Durden decomposition	Surface Scattering (P_S), Double Bounce Scattering (P_D), Volume Scattering (P_V)
	Yamaguchi decomposition	Surface Scattering (P_S), Double Bounce Scattering (P_D), Volume Scattering (P_V), Helix Scattering (P_h)
H/A/$\overline{\alpha}$ decomposition		Eigenvalue(λ_1, λ_2, λ_3), Eigenvector (P_1, P_2, P_3), Polarization scattering entropy(H), Eigen component (β, δ, γ), Anisotropy(A, A_{12}), Shannon entropy(SE, SE_P, SE_I), Single bounce eigenvalues relative difference($SERD$), Double bounce eigenvalues relative difference($DERD$), Polarization fraction (PF), Polarimetric asymmetry (PA), Radar vegetation index (RVI), Pedestal height (PH), Alpha approximation ($\overline{\alpha}$), Consistency correlation coefficient(CCC), Covariance matrix diagonal elements (C_{11}, C_{22}, C_{33})
Other parameters		Span of coherency matrix T3($Span$)、Polarization correlation coefficient(ρ_{12}, ρ_{13}, ρ_{23})

Separability Index

- Euclidean distance

$$D = \frac{|m_1 - m_2|}{\sqrt{\sigma_1^2 + \sigma_2^2}}$$

- K-S distance

$$d_n = d_K(F_n, F_0) = \sup_x |F_n(x) - F_0(x)|$$
$$= \max_i \left(\max(F_0(x_{(i)}) - \frac{i-1}{n}, \frac{i}{n} - F_0(x_{(i)}) \right)$$

L-band

	OW-Gi	OW-GiW	OW-Gw	OW-GwW	Gi-GiW	Gi-Gw	Gi-GwW	GiW-Gw	GiW-GwW	Gw-GwW	Ice Type
SE	0.26	1.54	3.57	2.88	1.79	3.26	2.53	5.42	5.06	1.16	2.75
SE_I	0.33	0.84	2.39	1.77	1.35	2.42	1.74	3.75	3.28	1.11	1.90
Span	0.28	0.78	2.09	1.61	1.17	2.00	1.49	3.13	2.80	0.84	1.62
$\bar{\alpha}$	0.61	0.64	2.06	1.05	1.80	1.87	0.68	3.63	1.80	0.65	1.48
λ_2	0.13	1.07	1.58	1.81	1.17	1.56	1.78	1.66	2.02	0.72	1.35
H	0.26	0.60	1.47	1.27	0.44	2.15	1.93	2.62	2.42	0.28	1.34
λ_3	0.24	1.42	1.55	1.57	1.04	1.54	1.50	1.60	1.72	1.04	1.32
SE_P	0.24	0.56	1.51	1.26	0.38	2.11	1.83	2.42	2.16	0.39	1.29
α_1	0.65	0.47	2.07	0.82	1.75	1.82	0.50	2.87	1.18	0.71	1.29
λ_1	0.17	0.64	1.52	1.24	1.05	1.49	1.21	1.81	2.17	0.93	1.22
$P_{V\_FREEMAN}$	0.16	1.24	1.42	1.32	1.05	1.44	1.36	1.49	1.58	1.01	1.21
p1	0.29	0.58	1.27	1.13	0.45	1.93	1.77	2.30	2.14	0.14	1.20

- Shannon entropy has the highest ice type discrimination ability.
- Good discrimination ability among sea ice types.
- Poor discrimination in OW-Gi separation and Gw-GwW separation.

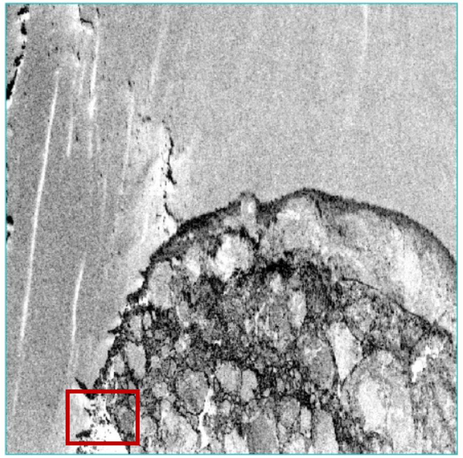

SE: ED=2.75

Clear differences between sea ice types

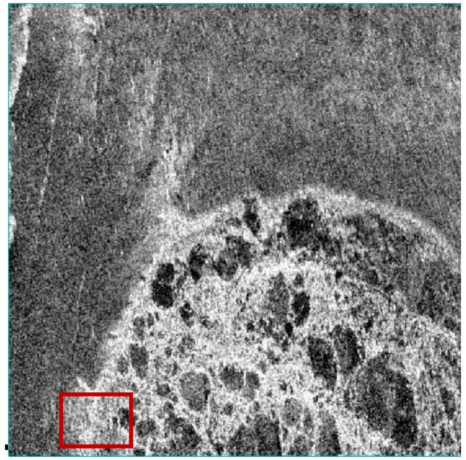

RVI: ED=1.10

OW and Gi are easily confused

S-band

	OW-Gi	OW-GiW	OW-Gw	OW-GwW	Gi-GiW	Gi-Gw	Gi-GwW	GiW-Gw	GiW-GwW	Gw-GwW	Ice Type
SE_I	1.80	2.49	3.25	4.27	0.94	1.96	3.24	1.07	2.12	0.79	2.19
SE	1.38	2.29	2.96	4.00	1.22	2.07	3.48	0.81	1.92	0.99	2.11
Span	1.67	2.35	2.98	3.95	0.84	1.69	2.77	0.92	1.85	0.69	1.97
$P_{V\_FREEMAN}$	1.49	2.19	1.95	2.95	1.03	1.49	2.48	1.01	1.96	0.72	1.73
λ_1	1.77	2.18	1.83	2.63	0.72	1.34	2.12	1.05	1.79	0.52	1.59
λ_2	1.22	1.81	1.96	2.72	0.89	1.48	2.30	0.93	1.79	0.80	1.59
λ	1.78	2.21	1.82	2.63	0.67	1.33	2.09	1.06	1.79	0.50	1.59
$P_{V\_Yamaguchi}$	1.18	1.67	1.73	2.43	0.68	1.38	2.04	1.08	1.71	0.43	1.43
λ_3	0.21	1.56	1.32	2.51	1.53	1.27	2.50	0.18	1.38	1.07	1.35

- Intensity component of shannon entropy has the highest ice type discrimination ability.
- Good discrimination ability between OW and sea ice.
- Poor discrimination in GiW-Gw separation and Gw-GwW separation.

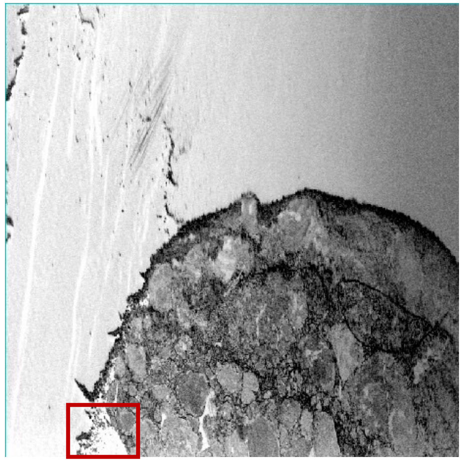

SE_I: ED=2.19

Except for Gw-GwW, other sea ice types vary significantly

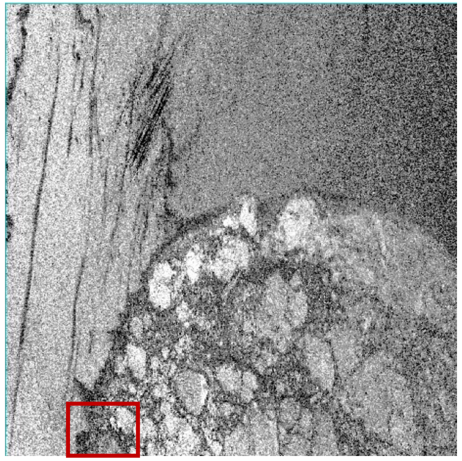

β: ED=0.83

OW and GI perform similarly

C-band

	OW-Gi	OW-GiW	OW-Gw	OW-GwW	Gi-GiW	Gi-Gw	Gi-GwW	GiW-Gw	GiW-GwW	Gw-GwW	Ice Type
SE	3.96	4.39	4.46	6.67	0.42	0.86	3.18	0.52	2.88	1.87	2.92
SE_I	4.14	4.81	4.28	6.90	0.60	0.68	3.00	0.20	2.56	1.73	2.89
Span	3.92	4.54	4.05	6.42	0.55	0.63	2.68	0.18	2.25	1.58	2.68
λ_3	1.76	1.76	1.73	2.40	0.22	0.95	2.06	0.80	1.99	1.51	1.52
$P_{V\_FREEMAN}$	1.69	1.72	1.69	2.37	0.30	0.90	2.01	0.67	1.90	1.47	1.47
$\overline{\alpha}$	1.18	0.19	2.23	2.10	1.24	1.42	1.17	2.41	2.36	0.42	1.47
λ_2	1.66	1.87	1.23	2.67	0.21	0.62	2.23	0.51	2.15	1.55	1.47
$P_{V\_Yamaguchi}$	1.59	1.67	1.70	2.17	0.21	0.91	1.85	0.75	1.79	1.38	1.40
λ_1	1.74	2.28	0.89	2.64	0.63	0.38	2.02	0.12	1.70	1.14	1.35
λ	1.72	2.27	0.86	2.65	0.65	0.38	2.04	0.11	1.70	1.12	1.35
α_1	0.84	0.00	2.30	1.51	0.92	1.70	1.00	2.40	1.56	0.44	1.27
C_{22}	1.49	1.58	1.39	1.83	0.25	0.75	1.56	0.60	1.49	1.14	1.21

- Shannon entropy has the highest ice type discrimination ability.
- Good discrimination ability between OW and sea ice.
- Poor discrimination in Gi-GiW separation and Gi-Gw separation.

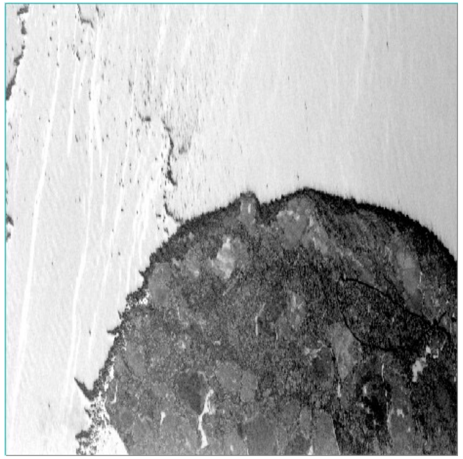

SE: ED=2.92

Clear contrast between OW and sea ice

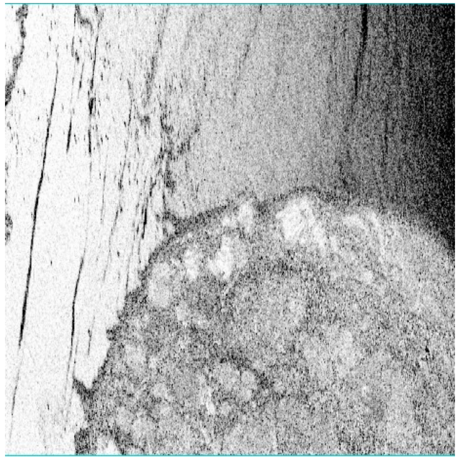

PF: ED=0.55

Almost indistinguishable between sea ice types.

Sea ice classification based on multi-band and multi-polarization features

- Extracting polarization features using multiple polarization decomposition methods
- Constructing a feature set based on separability index.
- Combining recursive feature elimination with various classifiers to discuss and obtain the optimal feature set.

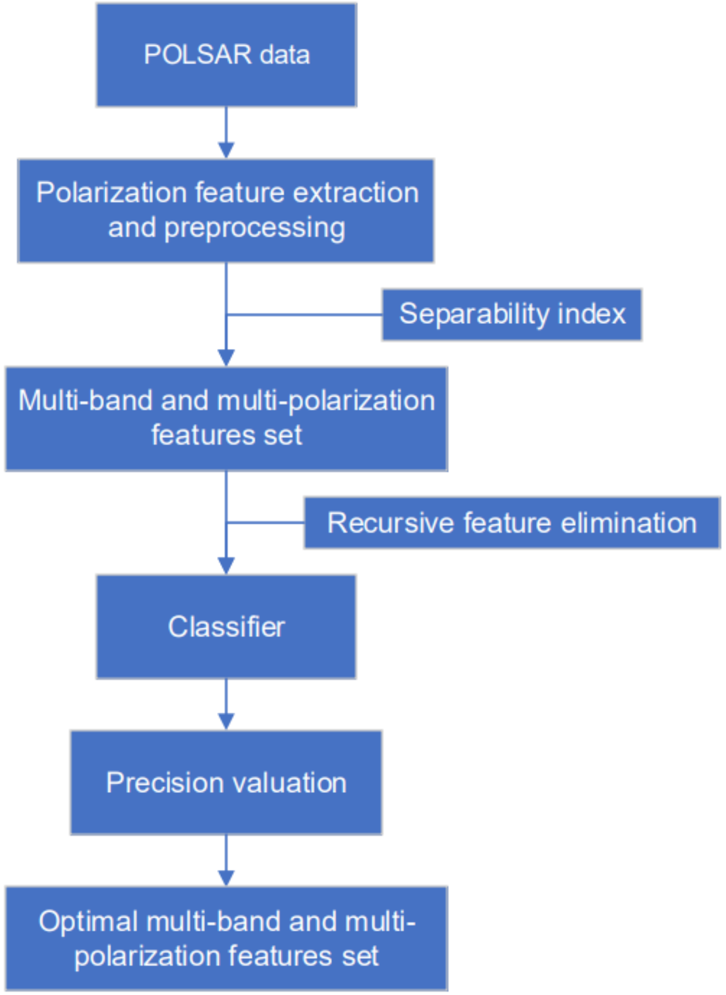

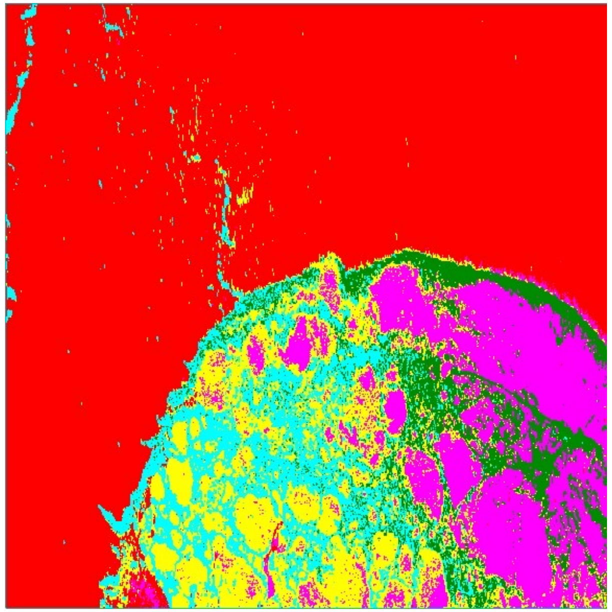

Proposed method

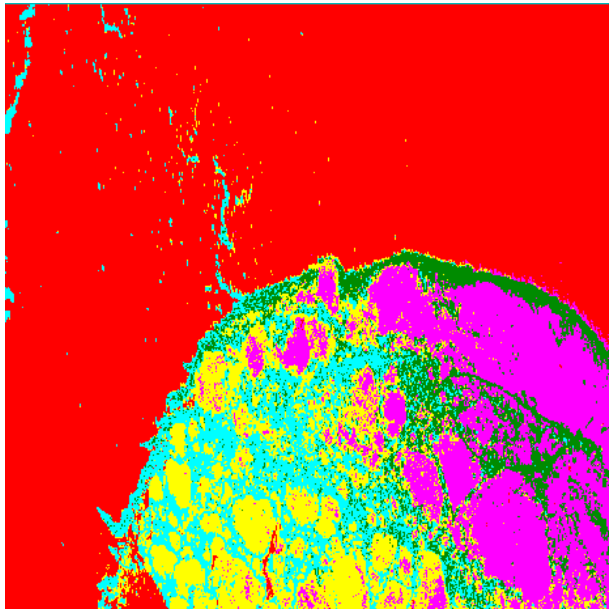

PCNN

	OW	Gi	Giw	Gw	GwW
OW	5250176	6199	7009	2526	10
Gi	31086	956218	78045	30439	27974
Giw	15138	37394	1104166	0	43807
Gw	2982	38471	0	787046	4309
GwW	48	6423	924	94268	475342
Uers acc	99.70	85.09	91.98	94.51	82.38
Overall acc/Kappa	95.26%/0.9222				

	OW	Gi	Giw	Gw	GwW
OW	5255513	9649	10555	1045	10
Gi	28226	871390	103412	38002	21304
Giw	412	75157	1074227	7	81564
Gw	15815	76717	29	746596	34223
GwW	94	11792	1921	128629	414341
Uers acc	99.60%	82.03%	87.24%	85.55%	74.42%
Overall acc/Kappa	92.91%/0.8837				

Operational sea ice mapping combining C- and L-band SAR imagery

- European ice services, Canadian ice service, and International Ice Patrol judged the gain of using L-band SAR images in addition to C-band data (ESA-funded project supported by JAXA and the International Ice Charting Working Group)
- Automatic classification of combined C- and L-band data were tested.
- Alignment of L- and C-band images acquired at different times was investigated.
- Gain of using L-band in addition:

+ earlier detection of fractures and of fast ice breakup
+ easier first-year / multi-year ice discrimination during the melt season
+ better discrimination of thin and thick ice
+ L-band is less sensitive to wind and sea state (=> iceberg detection)
+ Icebergs inside sea ice are easier to detect

2. Sea ice surface and bottom morphology observation with SAR data

Objective

- Does a correlation exist between sea ice surface deformation and bottom morphology?
- Is it possible to use SAR to invert sea ice surface deformation?
- Can SAR backscattering be correlated with the bottom morphology of ice?

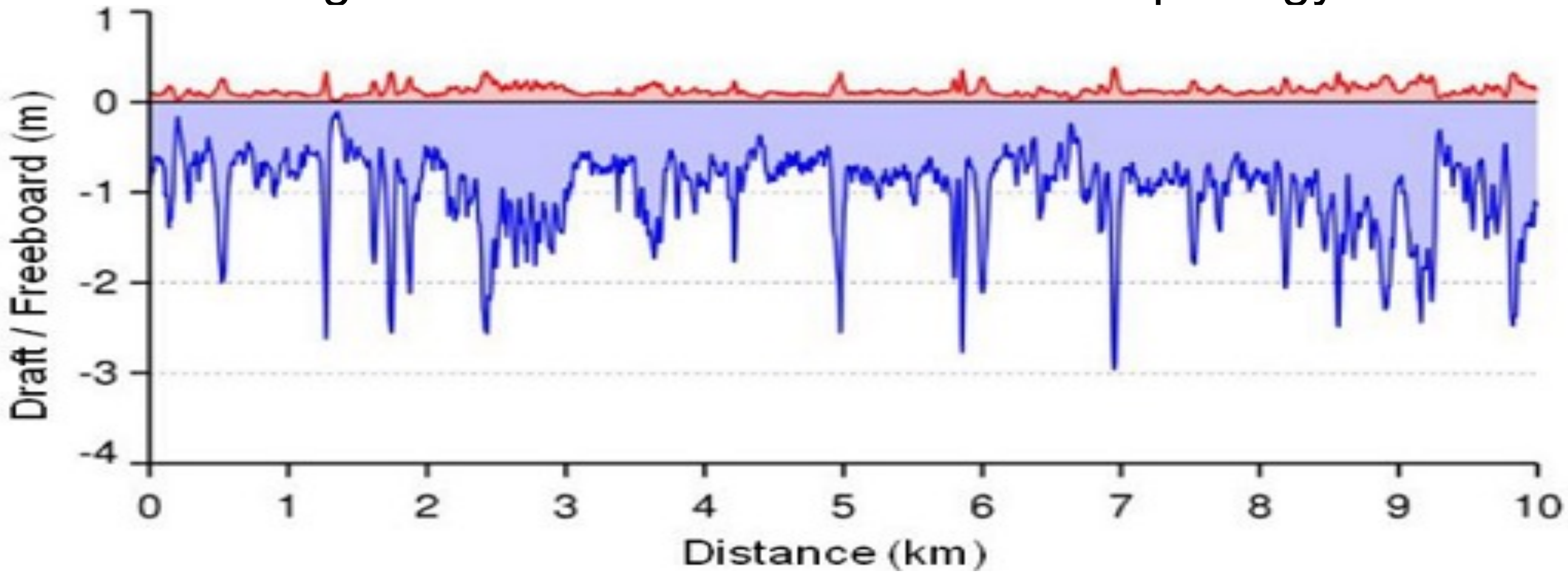

Answering the above questions is very useful for sea ice thickness retrieval from SAR.

■ Data

➢ Test site: Labrador coast

➢ Time: 19–20 March 2011

➢ In situ: Airborne HEM data

➢ SAR: RADARSAT-2 Quad-Pol data

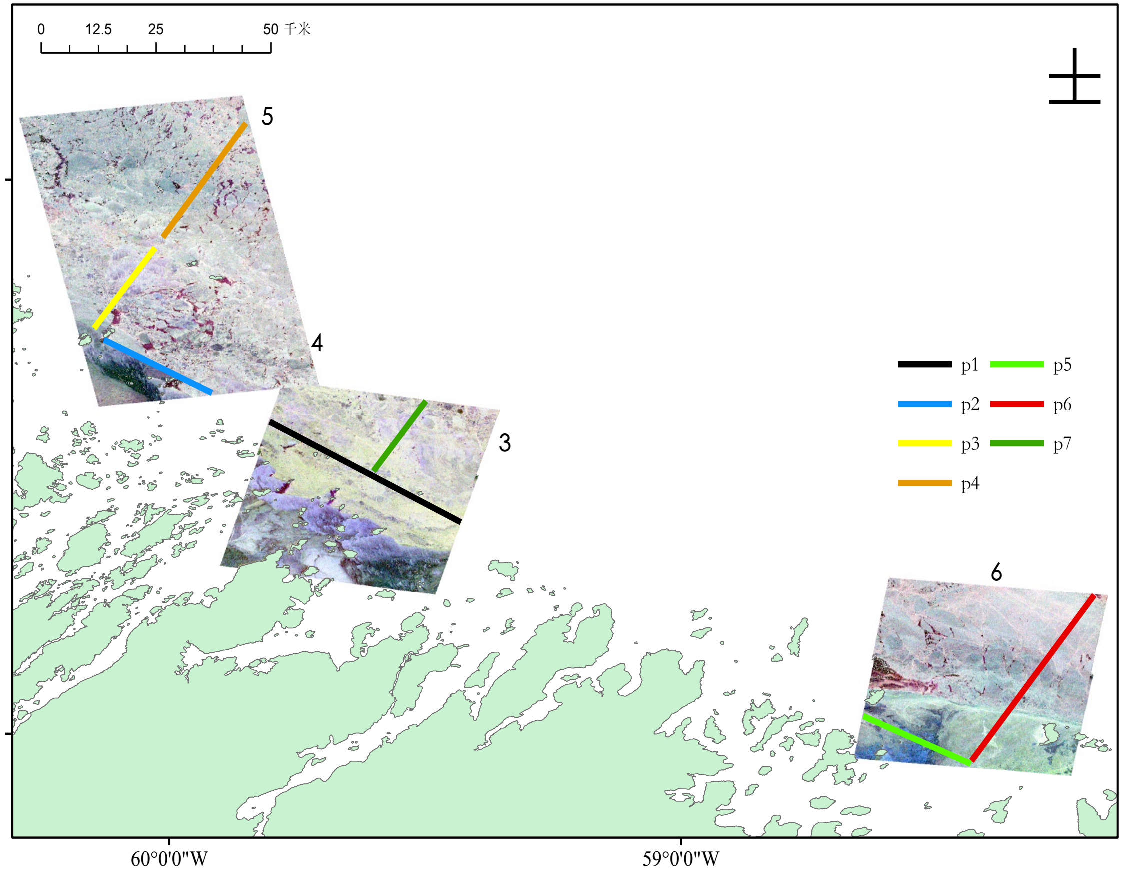

RADARSAT-2 PolSAR data were acquired nearly coincident with the airborne survey flights, with a maximum time difference of 4 hours.

Airborne HEM data can provide sea ice surface and bottom morphology

HEM	Data	Accuracy
Laser altimeter	Height of the snow surface	±1.5 cm
		±1.5 cm
Ground-penetrating radar	Snow depth	±5cm

- Ice-plus-snow thickness = EM - Laser
- Sea-ice thickness = EM - Laser – GPR
- Surface Morphology extracting from Laser
- Bottom Morphology extracting from EM

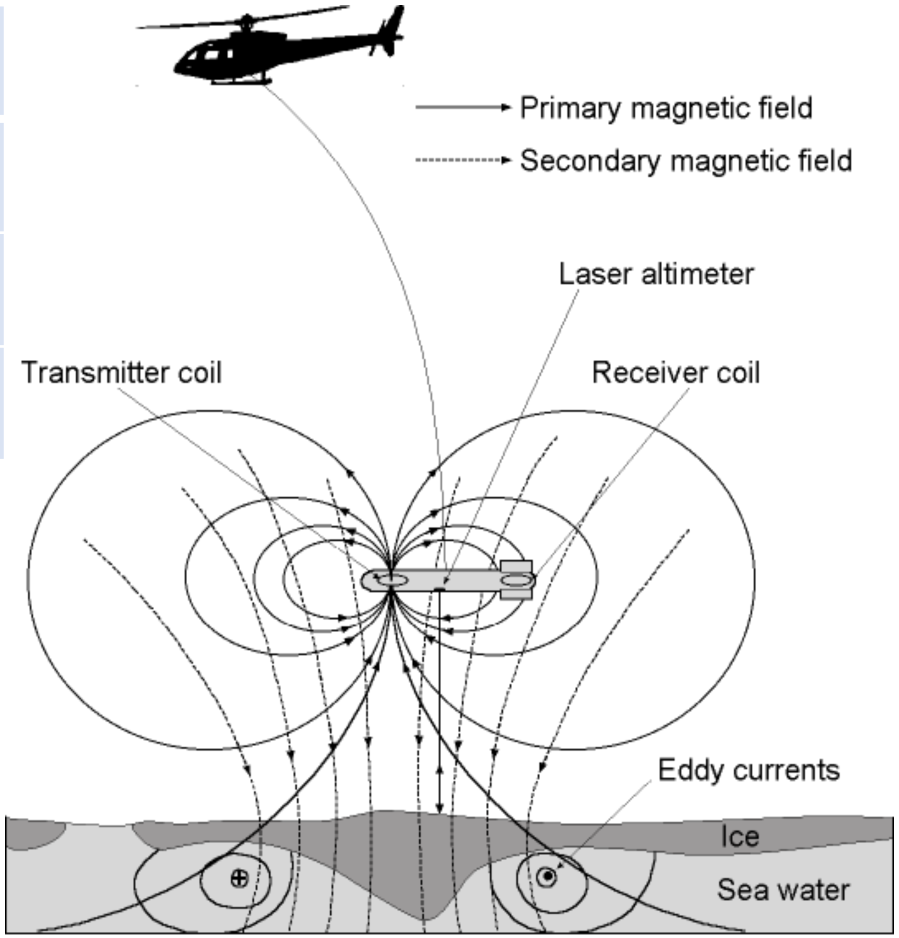

The parameters of surface and bottom morphology

Seven parameters are employed to describe both surface and bottom deformation

① Root-mean-square height (σ_h)

② Height skewness (h_{sk})

③ Height kurtosis (h_{ku})

④ Average slope (S)

⑤ Root-mean-square slope (σ_r)

⑥ Slope skewness (R_{sk})

⑦ Slope kurtosis (R_{ku})

$$\sigma_h = \sqrt{\frac{1}{n}\sum_{i=1}^{n}\left(h_i - \bar{h}\right)^2} \qquad \sigma_r = \sqrt{\frac{1}{n-1}\sum_{i=1}^{n-1}(S_i - \bar{S})^2}$$

$$h_{sk} = \frac{1}{n\sigma_h^{\ 3}}\sum_{i=1}^{n}(h_i - \bar{h})^3 \qquad R_{sk} = \frac{1}{(n-1)\sigma_r^{\ 3}}\sum_{i=1}^{n-1}(S_i - \bar{S})^3$$

$$h_{ku} = \frac{1}{n\sigma_h^{\ 4}}\sum_{i=1}^{n}(h_i - \bar{h})^4, \sigma_h = Srms \qquad R_{ku} = \frac{1}{(n-1)\sigma_r^{\ 4}}\sum_{i=1}^{n-1}(S_i - \bar{S})^4$$

$$\bar{S} = \frac{1}{n-1}\sum_{i=1}^{\text{n-1}} S_i, S_i = \left|\frac{h_{i+1} - h_i}{x_{i+1} - x_i}\right|$$

Correlation analysis between PolSAR feature and ice surface roughness

- Only Root-mean-square height has a strong correlation with polarization features.
- 9 polarization features have correlations with sea ice surface Root-mean-square height exceeding 0.6.
- The HV to HH ratio has the highest correlation coefficient (R=0.688).

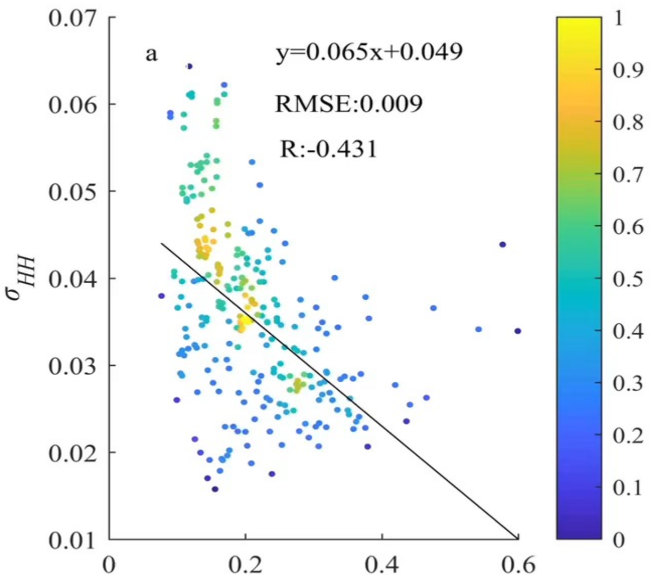

Root-mean-square height of sea ice surface/m

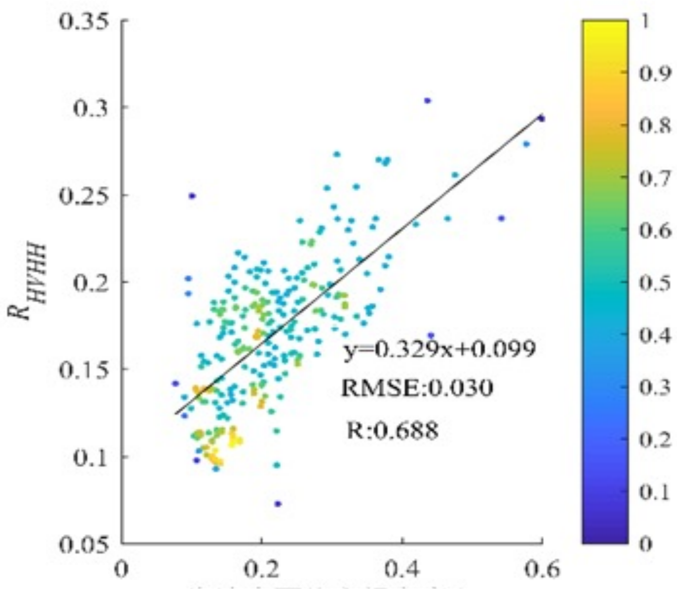

Root-mean-square height of sea ice surface/m

	σ_h	h_{sk}	h_{ku}	$\bar{S}$	σ_r	σ_{sk}	σ_{ku}
σ_{VV}	-0.241	0.100	0.095	-0.180	-0.156	0.049	0.042
σ_{VH}	0.167	0.059	0.024	0.196	0.146	-0.082	-0.103
σ_{HH}	-0.431	0.056	0.074	-0.409	-0.366	0.125	0.139
A	-0.367	0.077	0.090	-0.332	-0.269	0.156	0.158
A_{12}	-0.550	-0.039	0.016	-0.551	-0.476	0.133	0.179
PA	-0.261	-0.080	-0.040	-0.286	-0.261	0.024	0.064
$(1-H)(1-A)$	-0.455	-0.048	0.002	-0.458	-0.395	0.099	0.142
$(1-H)A$	**-0.602**	0.029	0.071	-0.579	-0.493	0.195	0.228
$H(1-A)$	**0.668**	-0.033	-0.081	**0.639**	0.535	-0.213	-0.247
H	**0.631**	0.019	-0.038	**0.622**	0.533	-0.17	-0.218
SE	-0.288	0.110	0.094	-0.013	-0.013	0.036	0.019
SE_I	-0.052	0.101	0.107	-0.247	-0.213	0.100	0.102
SE_P	**0.636**	0.017	-0.039	**0.625**	0.538	-0.174	-0.224
λ_1	-0.407	0.069	0.084	-0.369	-0.325	0.112	0.123
λ_2	0.008	0.120	0.089	0.058	0.048	0.012	-0.016
λ_3	0.167	0.072	0.041	0.196	0.155	-0.063	-0.087
PH	**0.684**	-0.023	-0.076	**0.660**	0.551	-0.208	-0.244
PF	**-0.683**	0.023	0.076	**-0.658**	-0.551	0.210	0.246
ρ_{12}	-0.167	-0.022	-0.033	-0.165	-0.155	-0.037	-0.053
ρ_{13}	-0.520	-0.057	-0.003	-0.526	-0.463	0.106	0.157
ρ_{23}	-0.120	-0.103	-0.109	-0.114	-0.135	-0.111	-0.095
RVI	**0.683**	-0.023	-0.076	**0.658**	0.551	-0.210	-0.246
$SERD$	**-0.663**	0.033	0.087	**-0.641**	-0.53	0.213	0.245

■ Correlation analysis between sea ice surface roughness and bottom roughness

- The first-order roughness parameters have the strongest correlation between ice surface and bottom roughness.
- The correlation between sea ice surface and bottom roughness weakens for higher-order roughness parameters.

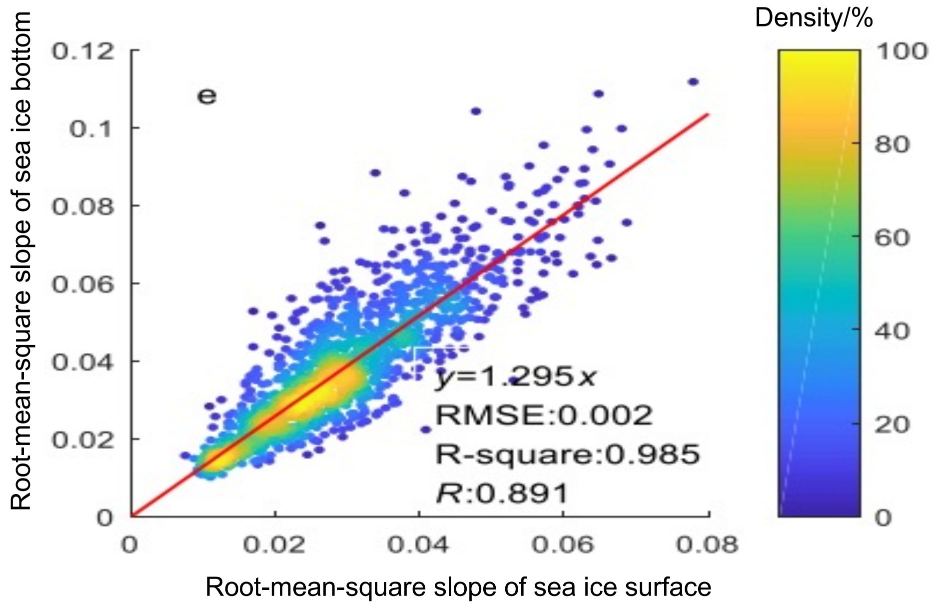

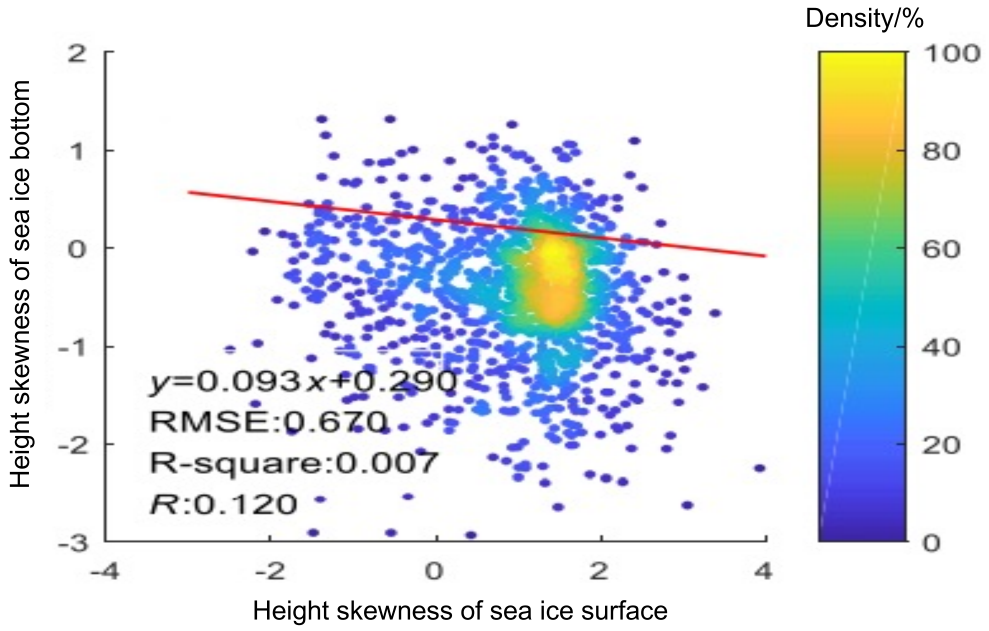

■ Correlation analysis between sea ice surface roughness and ice thickness

- The highest correlation between sea ice surface roughness and thickness is found at the average slope.
- There is no correlation between height kurtosis and sea ice thickness.

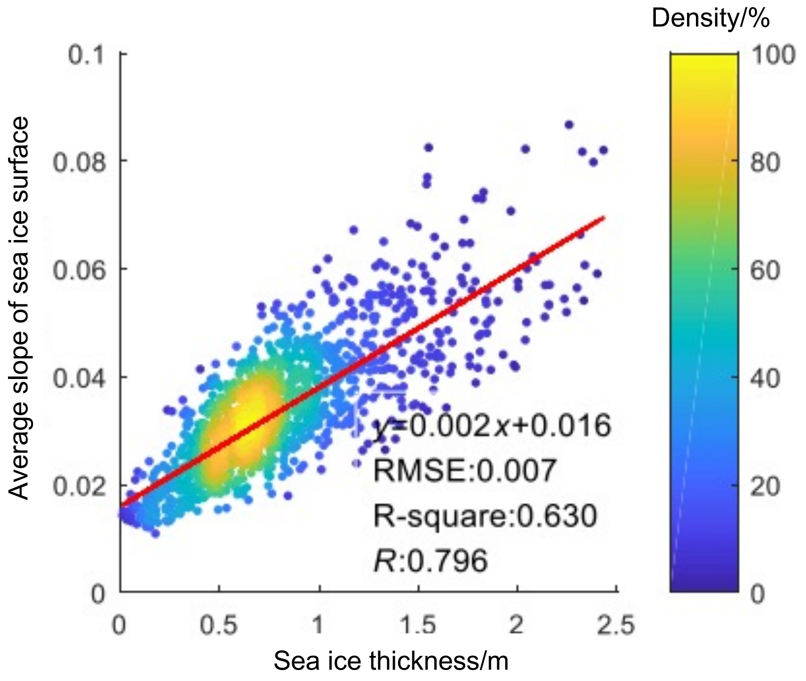

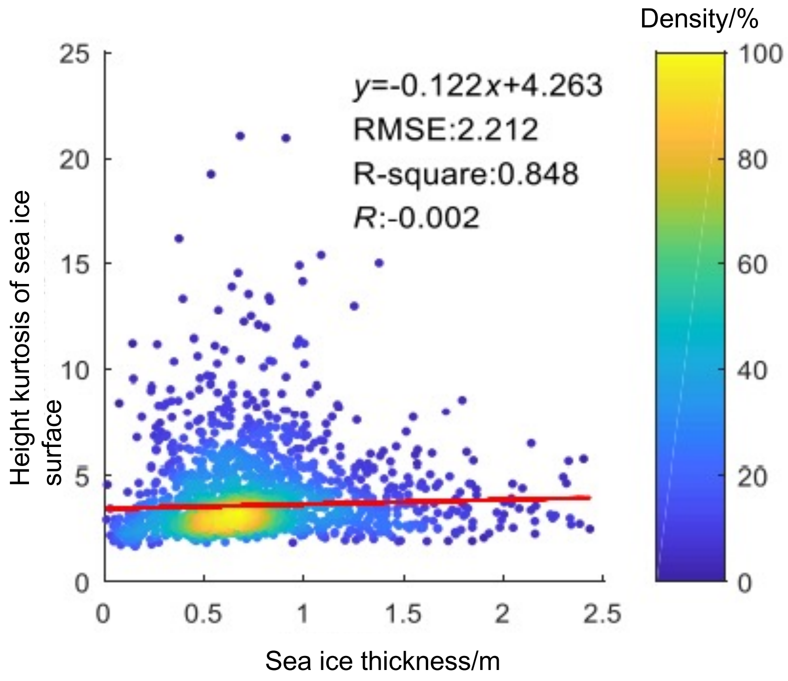

Parameters	R
σ_h	0.740
h_{SK}	-0.014
h_{ku}	-0.002
$\bar{S}$	0.796
σ_r	0.686
R_{sk}	-0.016
R_{ku}	-0.038

Correlation analysis between sea ice bottom roughness and ice thickness

- In comparison to the sea ice surface roughness, the bottom roughness values are larger and rougher.
- Similar with ice surface, the average slope has the highest correlation coefficient between sea ice bottom roughness and ice thickness.
- The slope skewness is the lowest.

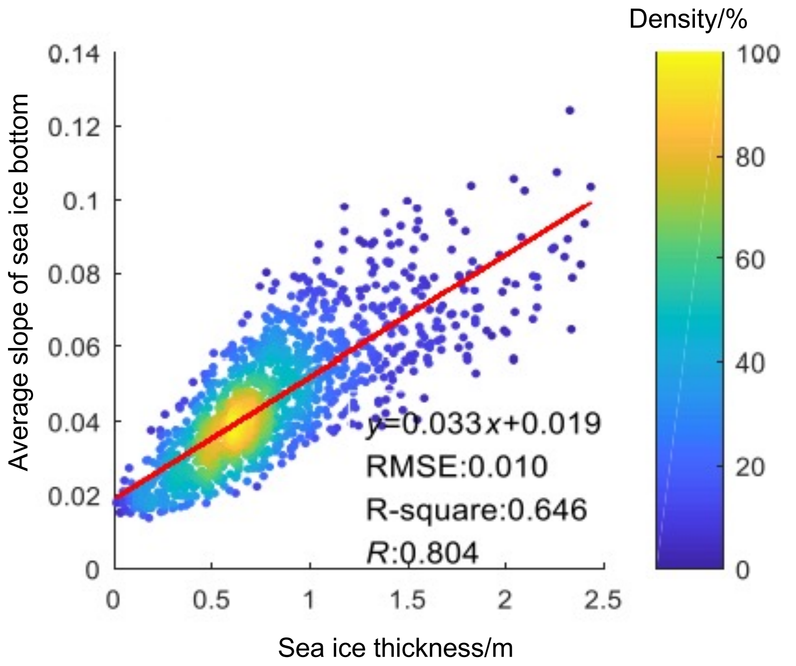

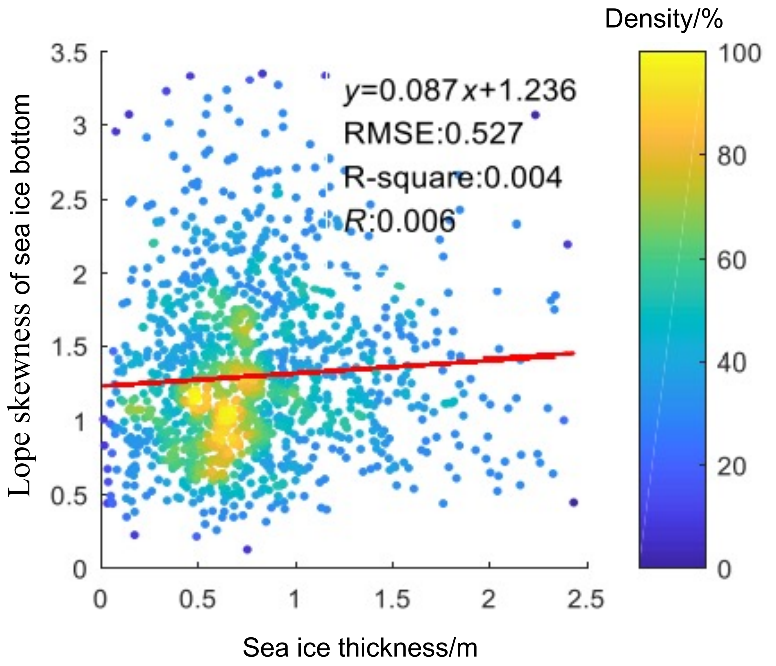

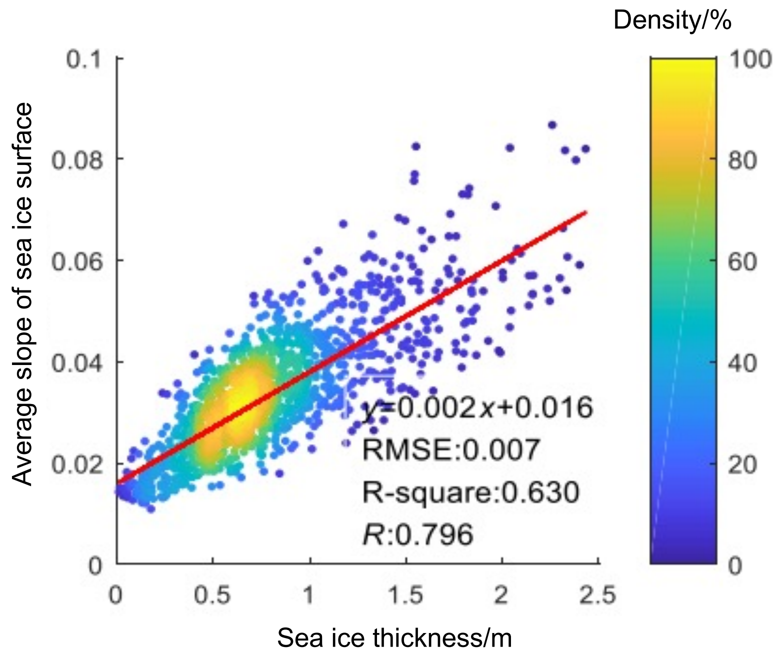

Correlation analysis between sea ice bottom roughness and ice thickness

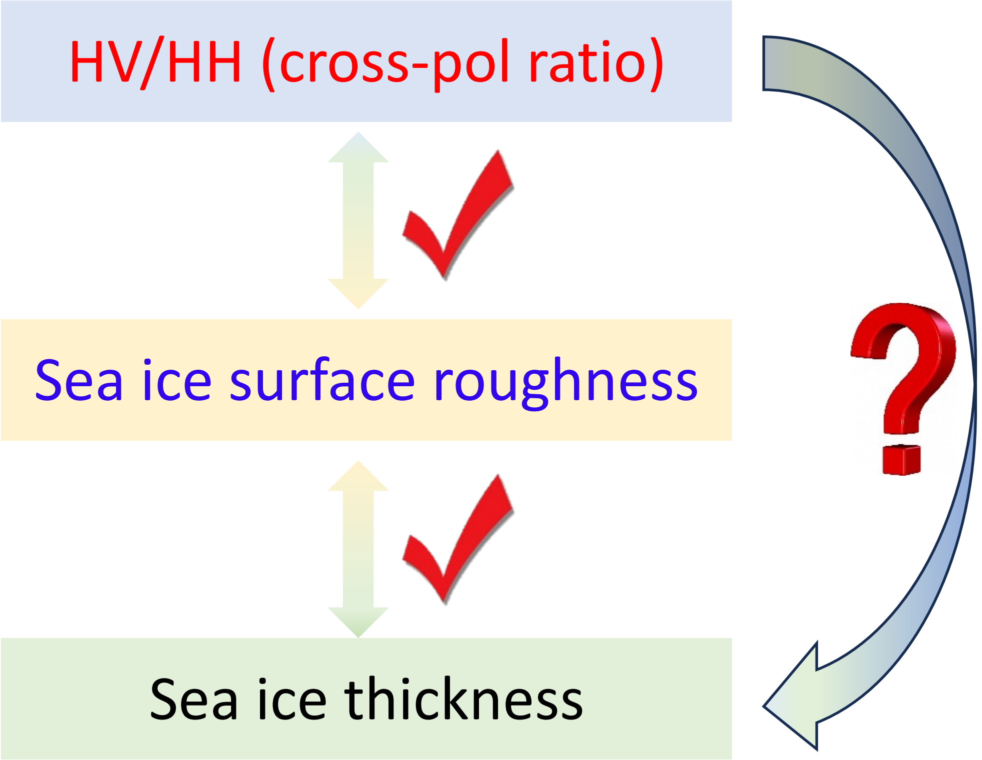

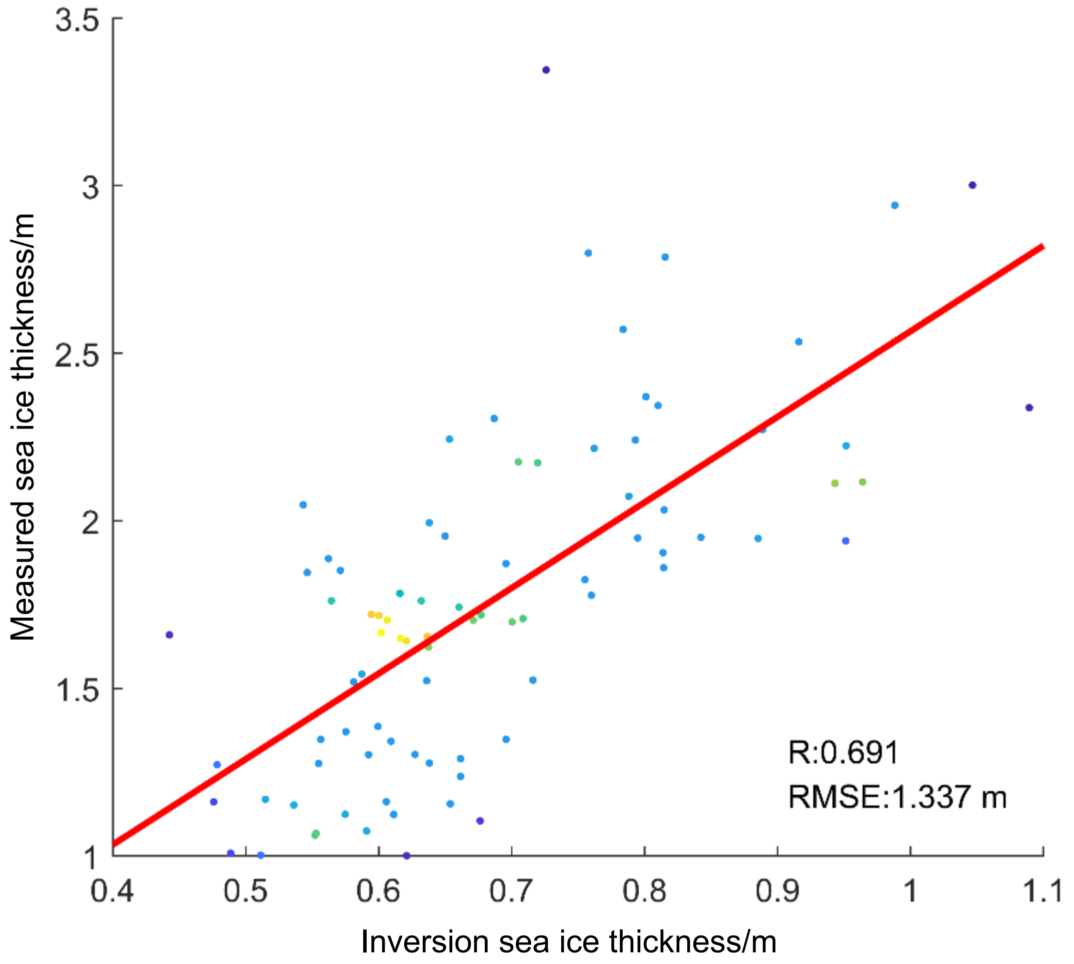

3. Sea ice drift extraction with FY-3D microwave radiometer data

Objective

- Developing a sea ice drift extraction method suitable for the FY-3D microwave radiometer.
- Evaluation with IABP buoy data, and the consistency between SSMIS, and AMSR2 sea-ice drift products.
- Analysis effects of different time intervals, frequencies, and SICs on the accuracy of ice drift.

Data

- FY-3D Microwave radiation imager
- DMSP SSMIS
- GCOM-W1 AMSR2

Auxiliary data

- NSIDC sea ice concentration: used for quality control
- IABP buoy: used to validation results

Methodology

A CMCC-based approach is used to generate sea ice drift products from gridded vertically and horizontally polarized Tb data from FY-3, HY-2, SSMIS, and AMSR2 radiometers.

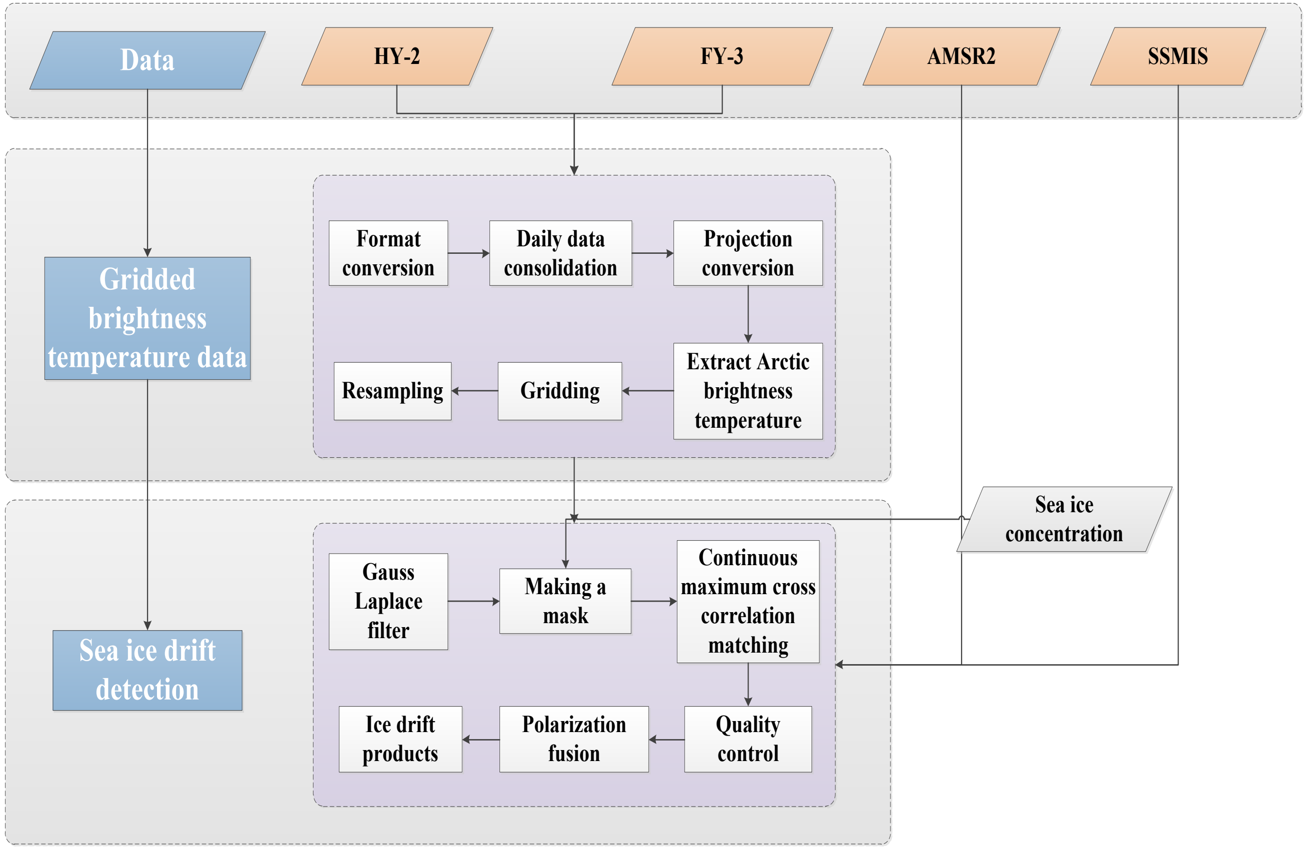

① Daily Tb data were merged, and the 37 GHz and 89 GHz data were gridded into 25 × 25 km and 12.5 × 12.5 km grid.

② Laplacian filtering was applied to reduce data noise, and exclude areas with SIC<15%.

③ CMCC with an 11 × 11 pixel slide window was used to retrieve sea ice drift.

④ A fusion method was used to average the H- and V- polarized sea ice drift vector results.

Effect of time interval on the accuracy of sea ice drift retrieval

Validation and comparison with IABP buoy data

Satellite	FY-3D		SSMIS		AMSR2	
RMSE	Speed (cm/s)	Direction (degree)	Speed (cm/s)	Direction (degree)	Speed (cm/s)	Direction (degree)
3 d	1.34	7.98	0.92	6.83	0.73	6.49
6 d	0.77	6.49	0.52	5.56	0.51	5.36
14 d	0.45	6.03	0.33	4.45	0.32	4.48

Satellite	FY-3D		SSMIS		AMSR2	
RE (%)	Speed	Direction	Speed	Direction	Speed	Direction
3 d	7.21	7.80	4.00	10.83	3.70	5.30
6 d	4.38	9.23	2.37	8.50	2.42	8.32
14 d	3.05	9.70	2.28	9.14	2.22	7.27

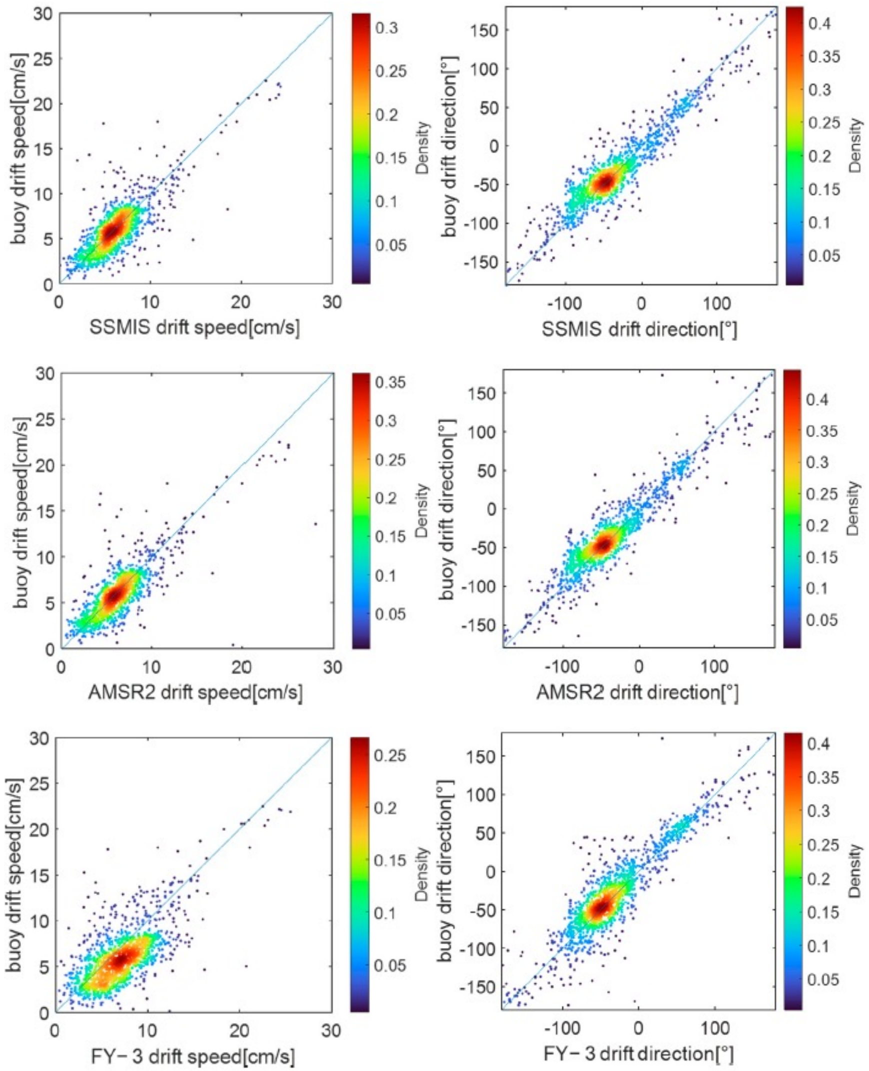

- Longer time intervals are associated with higher accuracy.
- However, considering the effect of the spatial and temporal resolution, an interval of 6 days is a good compromise.

Comparison of product accuracy at different frequency

Validation and comparison with IABP buoy data, the time interval is 6 d.

Satellite	FY-3D		SSMIS		AMSR2	
RMSE	Speed (cm/s)	Direction (degree)	Speed (cm/s)	Direction (degree)	Speed (cm/s)	Direction (degree)
37 GHz (January to February)	0.75	6.68	0.59	6.29	0.49	5.88
37 GHz (March to April)	0.77	6.42	0.51	5.56	0.51	5.36
89 GHz (January to February)	0.58	5.99	0.51	6.92	0.50	6.03
89 GHz (March to April)	0.70	7.13	0.49	5.85	0.53	6.14

- For FY-3, the accuracy was higher at 89 GHz than at 37 GHz.
- For SSMIS and AMSR2, the accuracy was slightly lower at 89 GHz.
- The low accuracy of the 37 GHz FY-3 product was probably related to outliers in the Tb data between orbits.

Intercomparison and consistency analysis of satellite-derived sea ice drift

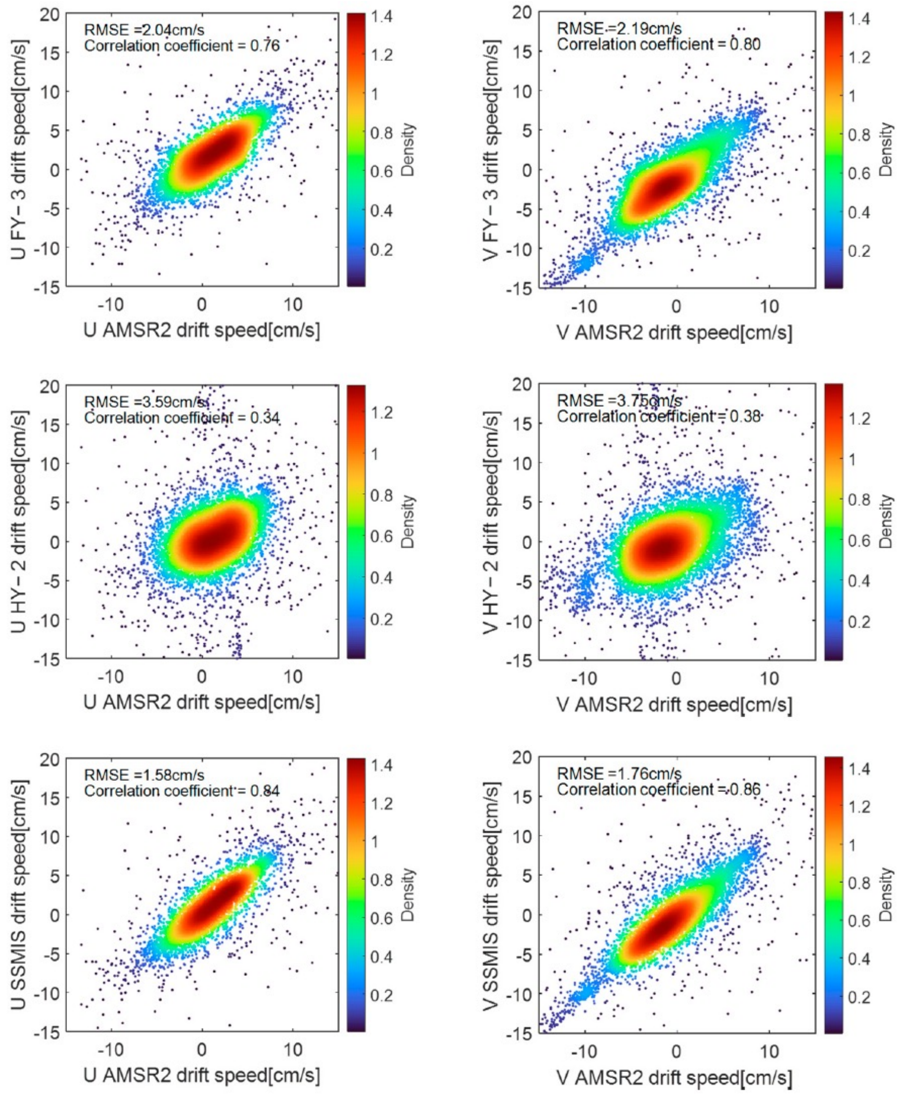

- 37 GHz :
  - R (0.77~0.89)
  - RMSE (1.19~1.99 cm/s)

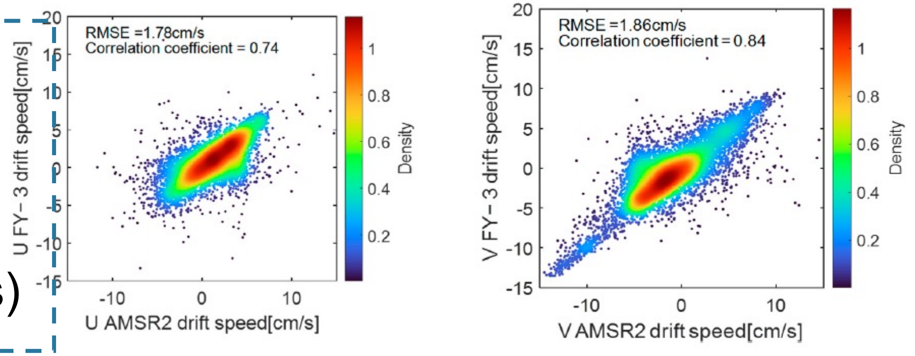

- 89 GHz :
  - R (0.68~0.81)
  - RMSE (1.67~2.13 cm/s)

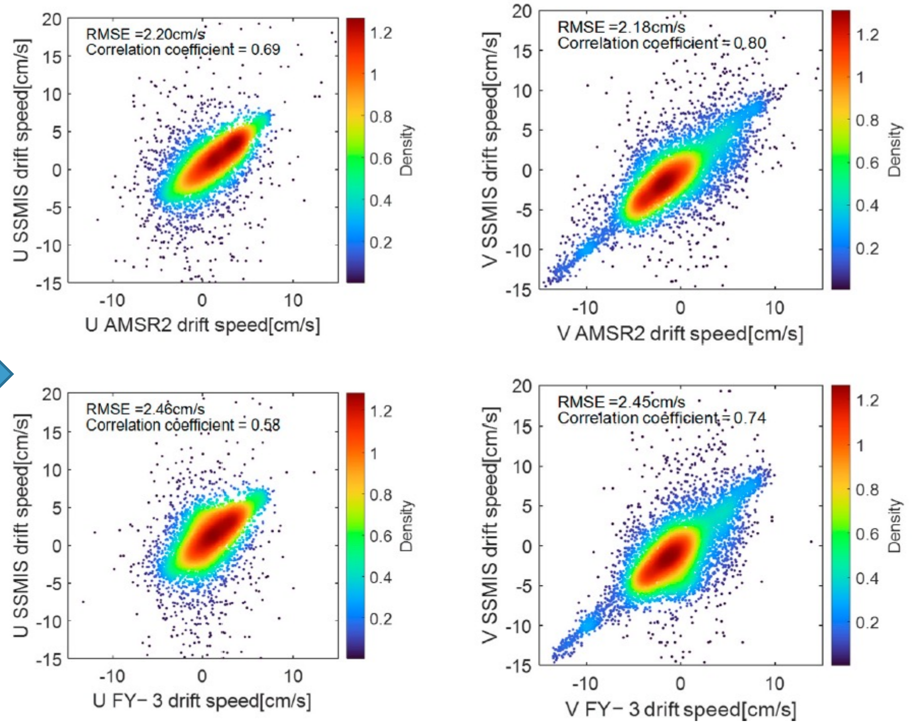

■ The effect of sea ice concentration on sea ice drift

- There is a negative correlation between ice speed differences and sea ice concentration.
- Speed differences are notably high for all products at concentrations of 80–90%, but they decrease at concentrations exceeding 90%.
- The smallest differences in drift speeds are observed between those retrieved from SSMIS and AMSR2.
- For concentrations below 70%, differences between drift speeds retrieved from FY-3 and those from AMSR2 remain small, but they become relatively large at concentrations of 70–90%.

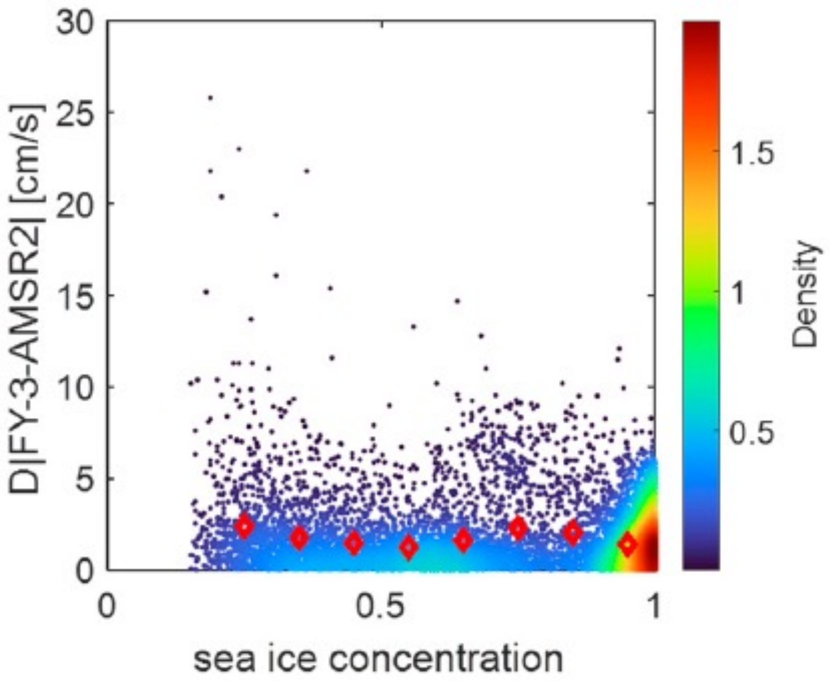

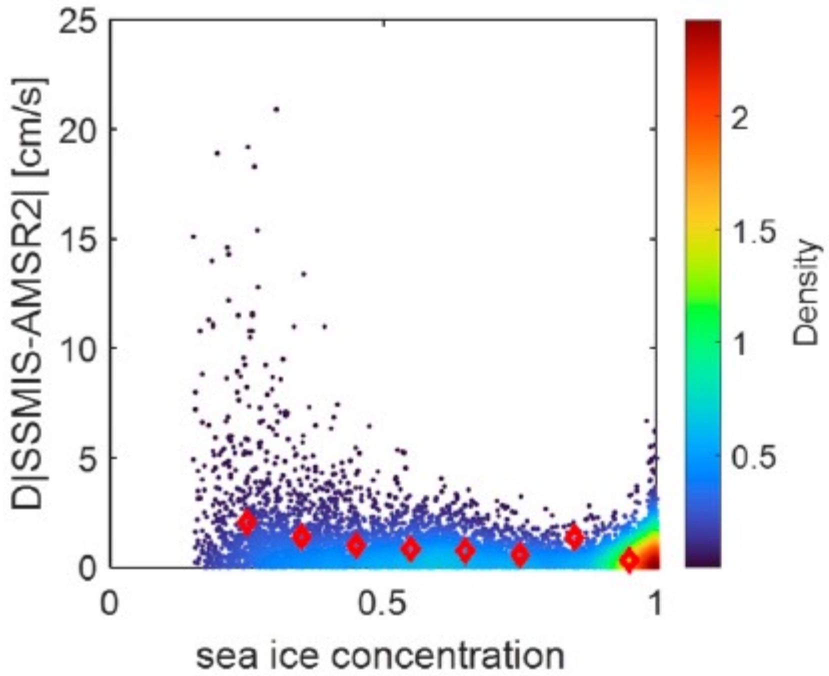

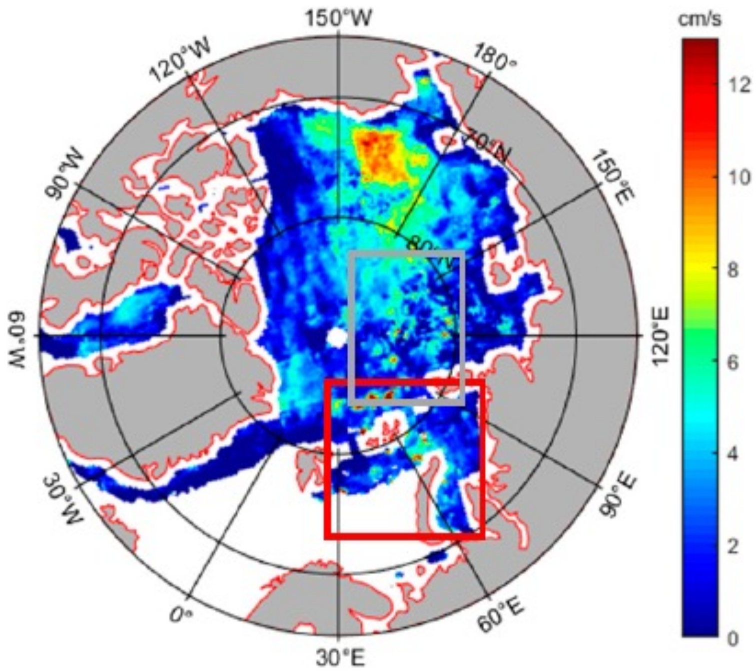

FY-3D ice drift speed

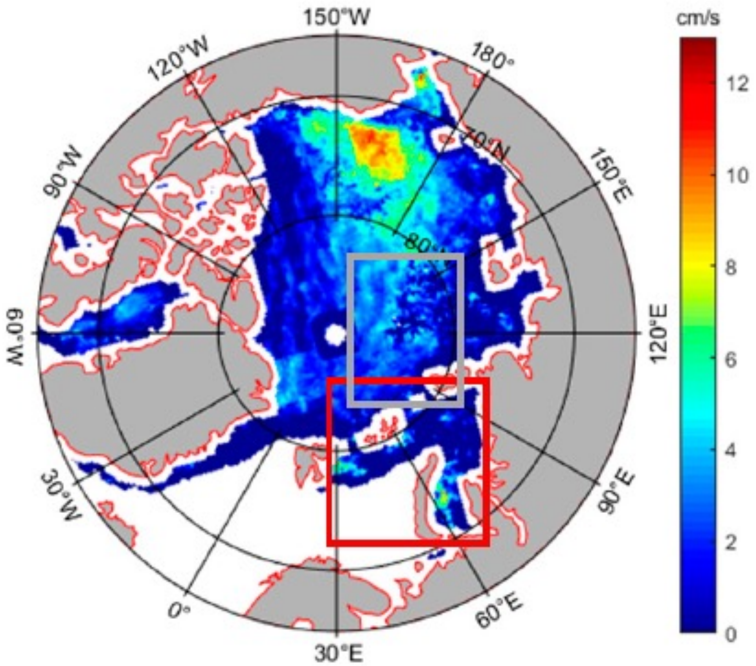

SSMIS ice drift speed

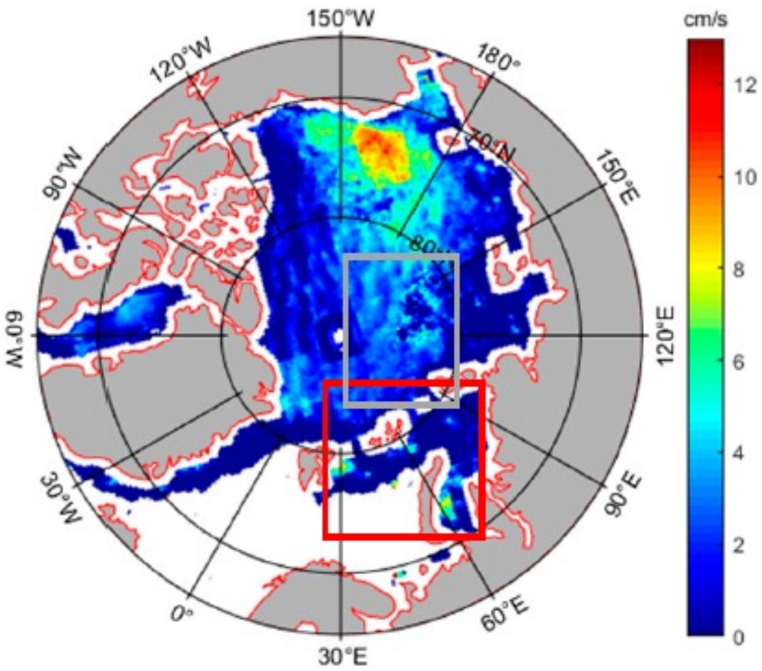

AMSR2 ice drift speed

- Our results showed that the four microwave radiometers provided relatively consistent measurements of sea ice drift.
- The largest differences were concentrated at the ice edge and between eastern Iceland and western Russia.

4. Snow depth retrieval over sea ice using microwave radiometer data

Objective

- Snow over sea ice controls energy budgets and affects sea ice growth and melting.
- Passive microwave radiometers can be used for basin-scale snow depth estimation at a daily scale.
- The Antarctic sea ice surface is covered by a thick layer of snow, and high-frequency signals of radiometer cannot completely penetrate the snow-load.
- The existing algorithm tends to underestimate the snow depth by approximately half of its actual value.

A new snow depth retrieval model was developed using low-frequency Tbs.

Data

- AMSR-E (2002-2011)
- AMSR2 (2011-2012)

AMSR-E

AMSR2

Auxiliary data

- Airborne OIB snow depth data
- ASPeCt shipboard observation data
- AADC in situ data

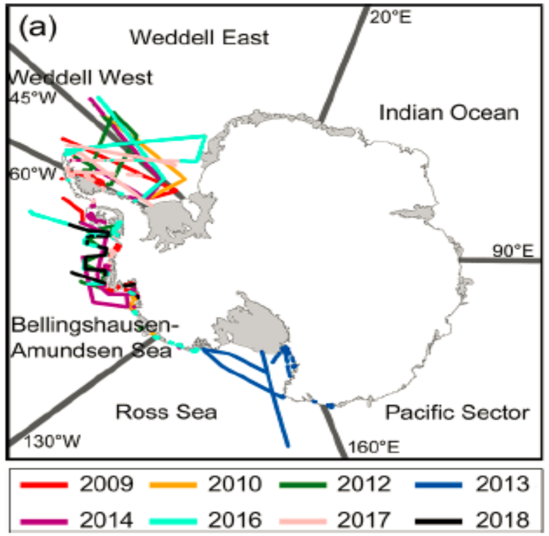

Spatial and temporal distribution of OIB data

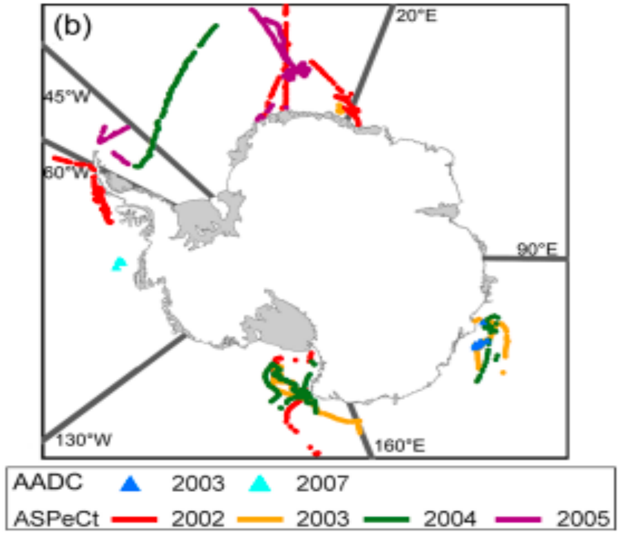

Spatial and temporal distribution of AADC and ASPeCt data

Methodology

- The vertical polarization GR at 19 and 37 GHz are commonly used to estimate of snow depth.
- 19 and 37 GHz, high-frequency, hardly penetrate snow load.
- 7 GHz, low-frequency, can penetrate snow cover at greater depth.

$$\mathrm{GR}(37/19)=\frac{Tb_{37}-Tb_{19}-k_1(1-C)}{Tb_{37}+Tb_{19}-k_2(1-C)}$$

$$k_1=Tb_{37,OW}-Tb_{19,OW}\qquad k_2=Tb_{37,OW}+Tb_{19,OW}$$

$$\mathrm{SD}\ (\mathrm{cm})=a+b\cdot GR(37/19)$$

$$\boxed{\mathrm{SD}_{\mathrm{GR}(37/7)}(\mathrm{cm})=26.7-411\cdot GR(37/7)}$$

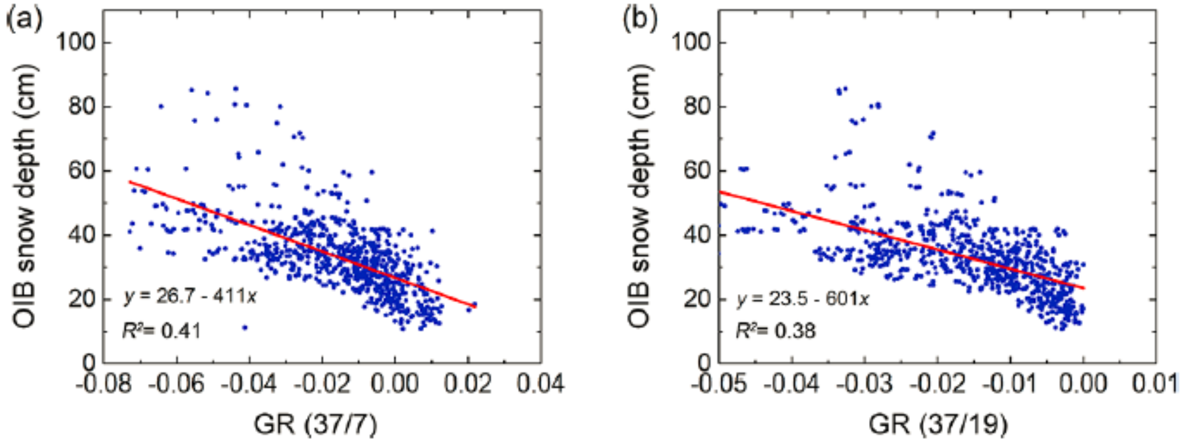

GR	RMSD (cm)	Correlation coefficient	Number of grid cells
GR(37/24)	9.22	−0.61	740
GR(37/19)	9.11	−0.62	
GR(37/11)	8.95	−0.64	
GR(37/7)	8.92	−0.64	
GR(24/19)	9.21	−0.61	
GR(24/11)	9.03	−0.63	
GR(24/7)	9.14	−0.62	
GR(19/11)	9.15	−0.62	
GR(19/7)	9.46	−0.58	
GR(11/7)	10.62	−0.41	
$\frac{\mathrm{GR}(37/19)+\mathrm{GR}(19/10)}{2}$	8.96	−0.64	

Self-evaluation of the proposed method

The regression coefficients of snow depth estimation equations based on OIB snow depth data in different years

Year	Intercept	Slope	Number of grid number
2009	25.4	-417	161
2010	27.2	-445	88
2012	28.3	-349	147
2013	23.8	-707	40
2014	25.4	-394	103
2016	27.3	-474	134
2017	33.8	-176	68
Apply all data	26.7	-411	740

- No obvious interannual variations could be found for either the slope or the intercept values.

The comparisons between the OIB snow depth and the snow depth estimates from our method and the Comiso method

	MD (cm)	MAD (cm)	RMSE (cm)	Correlation coefficient
Proposed	-1.55	6.84	9.23	0.62
Comiso	-19.15	19.15	21.26	0.60

- The proposed method has a good result by compared with OIB snow depth.

Comparison to AADC and ASPeCt data

	Comparison to AADC data		Comparison to ASPeCt data	
	Proposed method	Comiso method	Proposed method	Comiso method
MD (cm)	5.64	-14.47	8.62 (8.94)	-9.96 (-10.16)
MAD (cm)	10.77	17.08	13.80 (13.91)	13.11 (13.20)
RMSD (cm)	13.79	19.49	16.85 (16.85)	17.61 (17.61)
Correlation coefficient	0.42	0.40	0.13 (0.13)	0.19 (0.19)
Number of grid cells	15	15	264 (257)	273 (257)

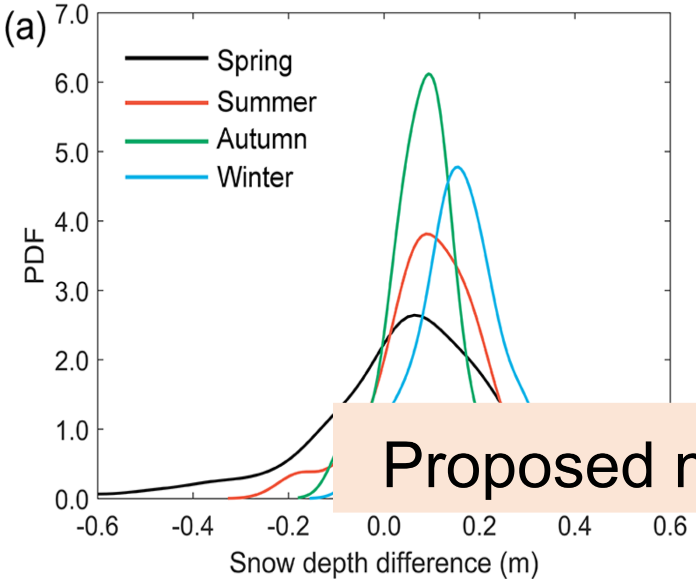

Snow depth differences:
Proposed method- ASPeCt

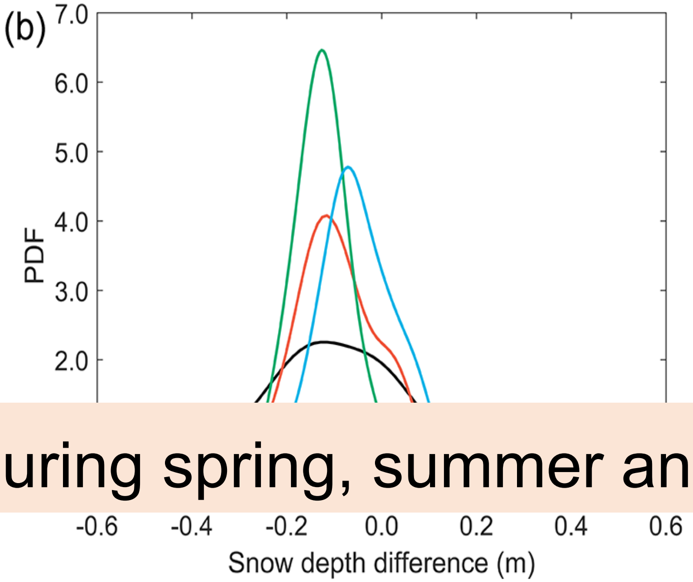

Snow depth differences:
Comiso method- ASPeCt

Proposed method was better during spring, summer and autumn

The uncertainty from estimation methods

Considering the sources of uncertainty: brightness temperatures, model coefficients, et al.

$$\sigma_{\mathrm{SD}} = \sqrt{\left(\frac{\partial \mathrm{SD}}{\partial a}\right)^2 (\sigma_a)^2 + \left(\frac{\partial \mathrm{SD}}{\partial b}\right)^2 \sigma_b^2 + b^2 \sigma_{GR}^2}$$

$$\sigma_{GR} = \sqrt{G_1^2 \sigma_{Tb_{v1}}^2 + G_2^2 \sigma_{Tb_{v2}}^2 + G_3^2 \sigma_{k_1}^2 + G_4^2 \sigma_{k_2}^2 + G_5^2 \sigma_c^2}$$

- The uncertainty of proposed method: 0~50 cm
- The uncertainty is large in the marginal zone and small in the interior; while is large in summer and small in winter.

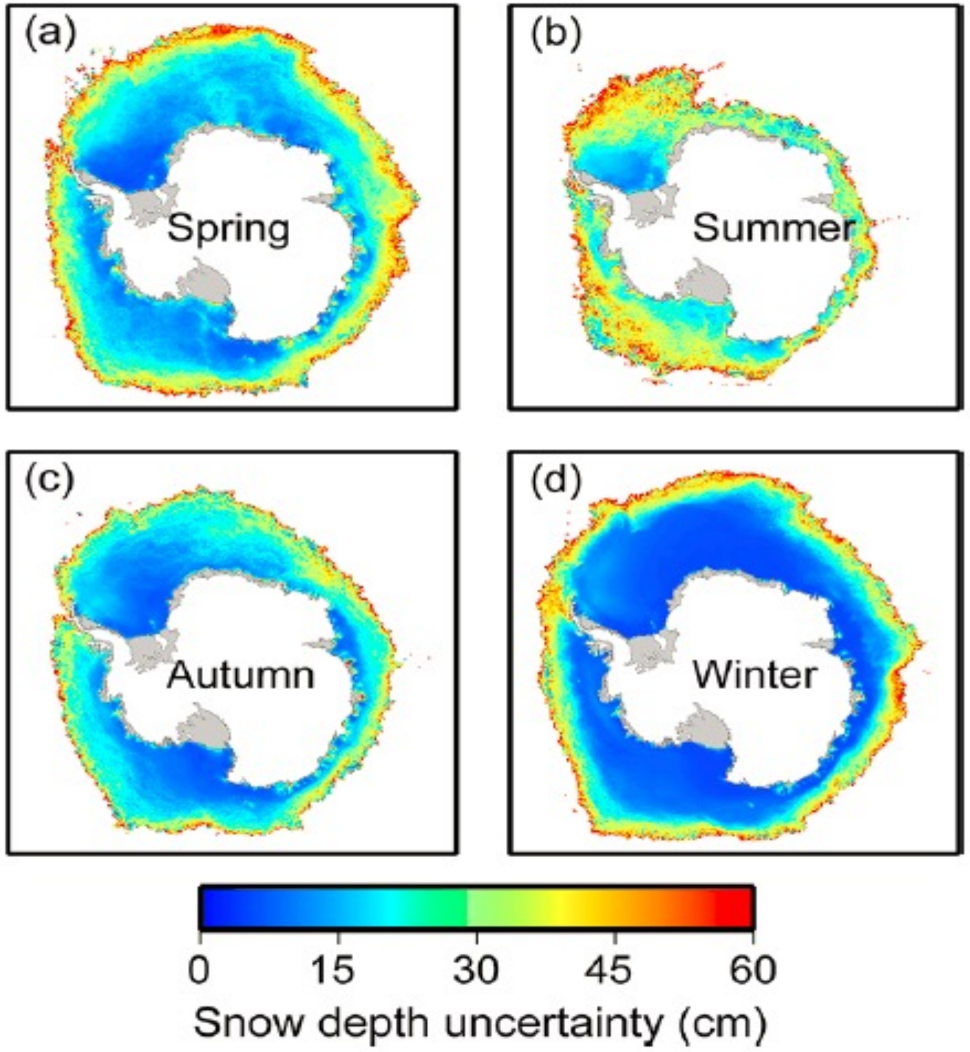

Data access

Antarctic Sea Ice Surface Snow Thickness Dataset (2002-2020), published in the National Tibetan Plateau Science Data Center https://doi.org/10.11888/Snow.tpdc.271653

Shen, X., Ke, C.-Q., et al. (2022). A new digital elevation model (DEM) dataset of the entire Antarctic continent derived from ICESat-2, *Earth Syst. Sci. Data*, 14, 3075–3089, https://doi.org/10.5194/essd-14-3075-2022.

5. Analysis of decadal changes of sea ice in the Bohai Sea with GOCI data

Objective

- The region surrounding the Bohai Sea is a important strategic economical circle.
- Sea ice seriously impacts ports, shipping, fishers, and marine operations around the Bohai Sea.
- Sea ice monitoring is an important task.

A long-term analysis helps us understand sea ice changes and climate change.

GOCI Data

- Satellite： Communication Ocean and Meteorological Satellite, Korea
- Launch: June 2010, Korea
- Orbit: Geostationary Orbit
- Spatial resolution: 500 m
- Imaging Time: 00:15 (UTC) ~07:45 (UTC), 8 images a daytime
- Band: 8 bands (6 visible, 2 NIR)

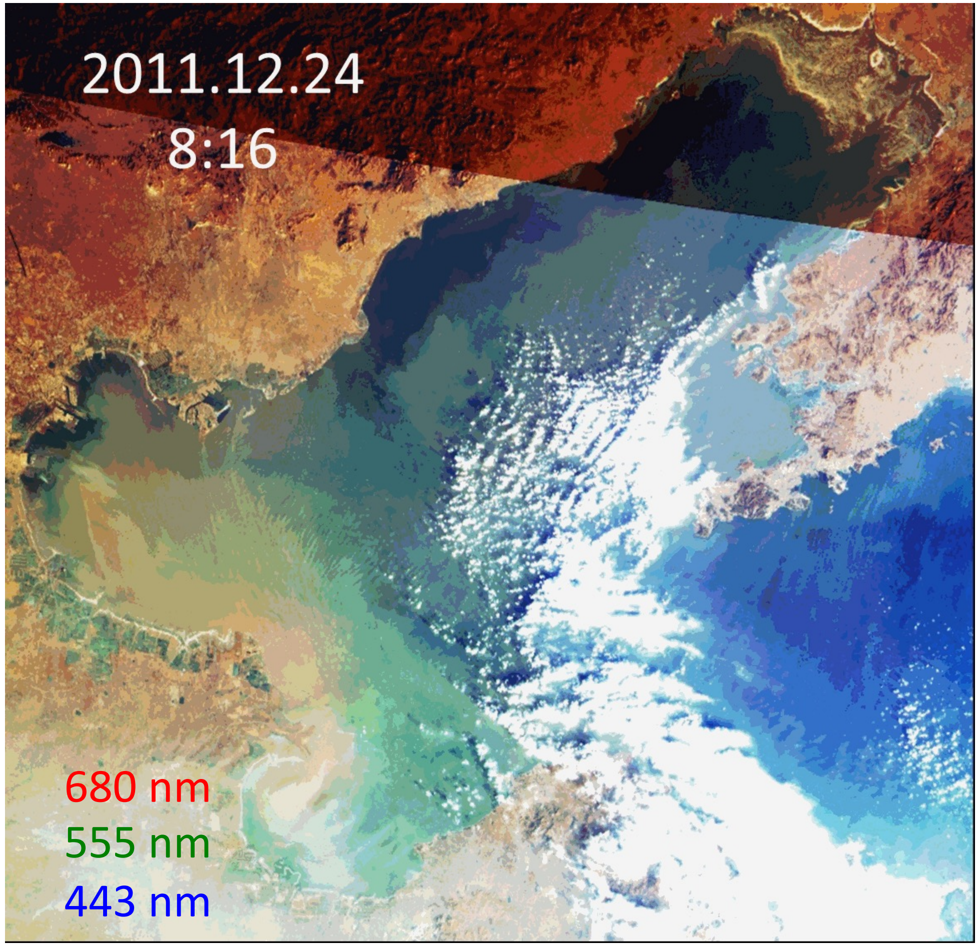

GOCI data can provide hourly sea ice observations with 500 m resolution.

Sea ice parameters extraction

Sea ice concentration

$$seaice_{con} = \frac{\alpha_{short} - \alpha_{sea}}{\alpha_{ice} - \alpha_{sea}}$$

Sea ice thickness

$$\alpha = \alpha_{\max}\left[1 - \frac{\alpha_{sea}}{\alpha_{\max}}\exp(-\mu h)\right]$$

Sea ice drift

MCC method

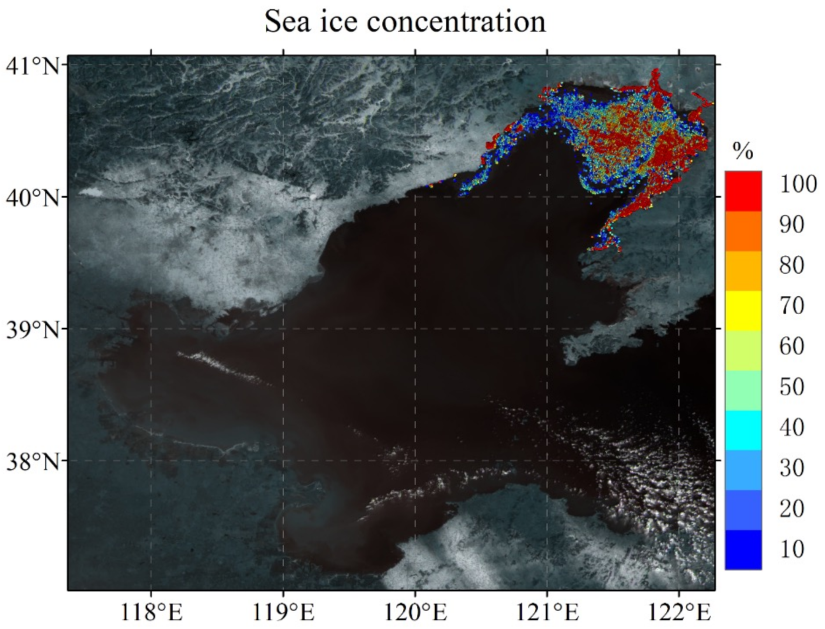

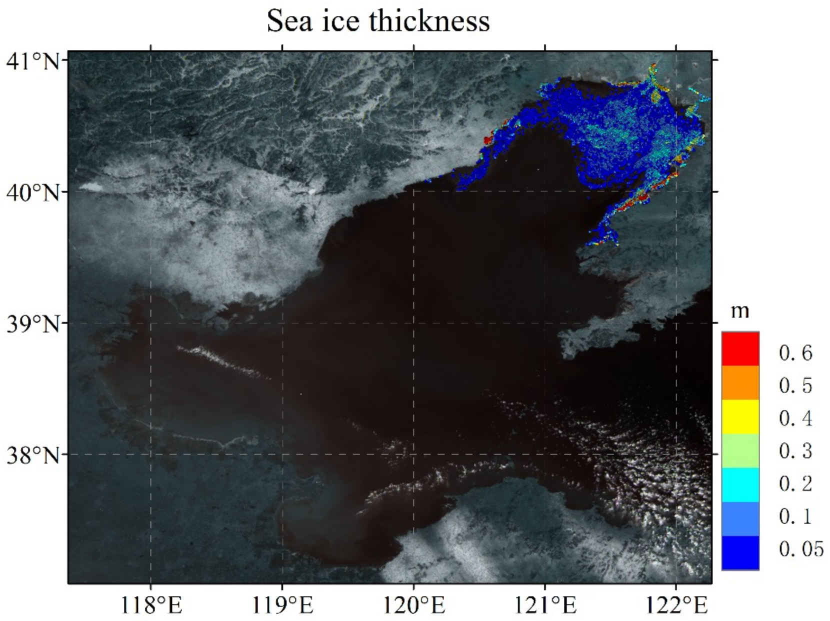

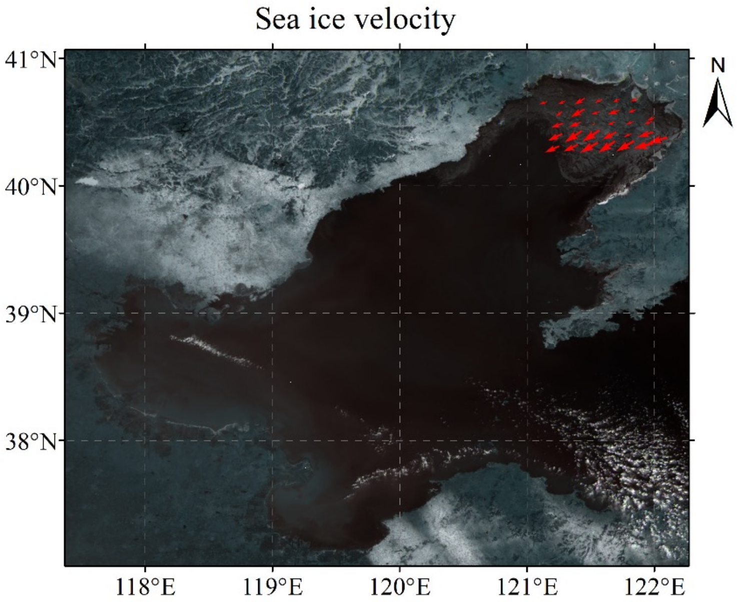

Decadal changes of sea ice area

Annual average sea ice area

-357.4 km^2/year

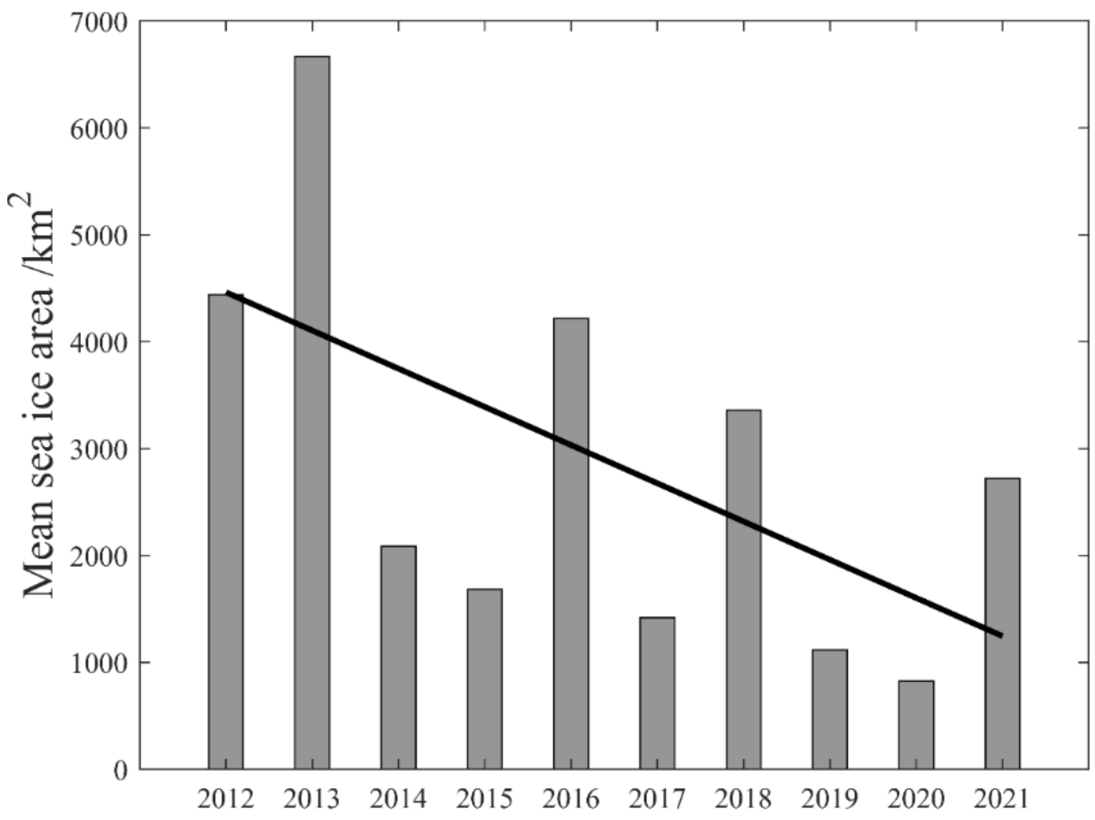

Annual maximum sea ice area

-1214.1 km^2/year

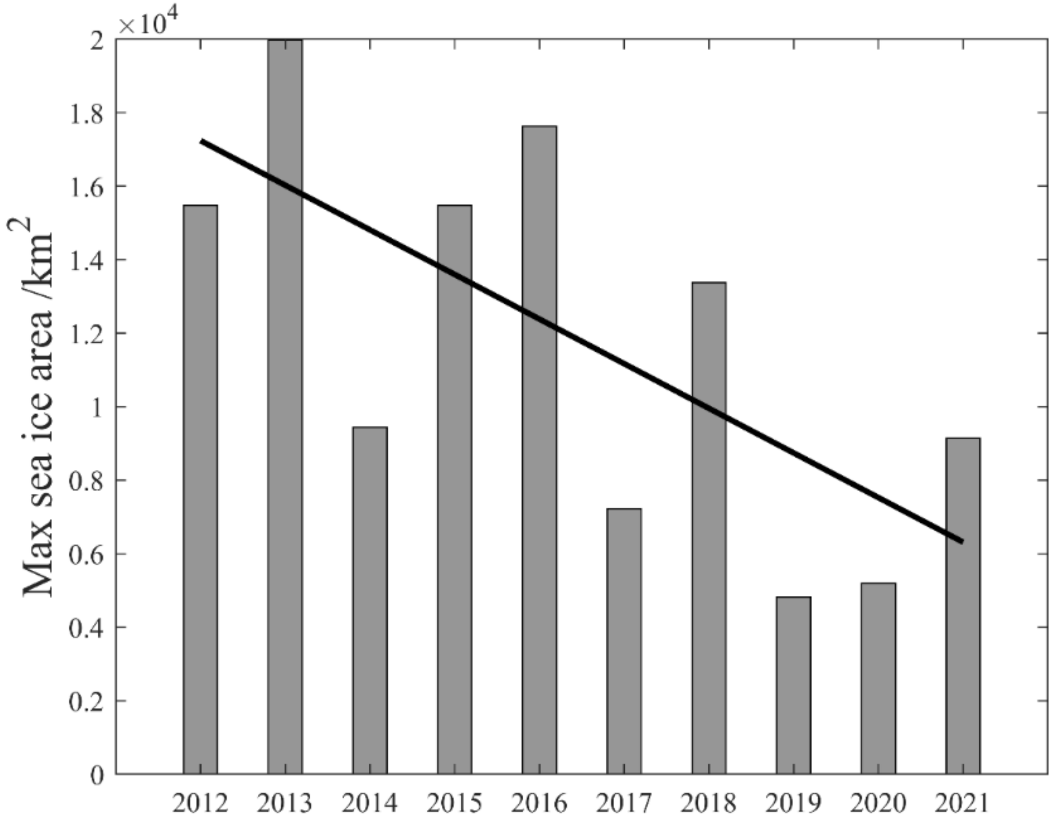

Decadal changes of sea ice thickness

Annual **average** sea ice thickness

-0.30 cm/year

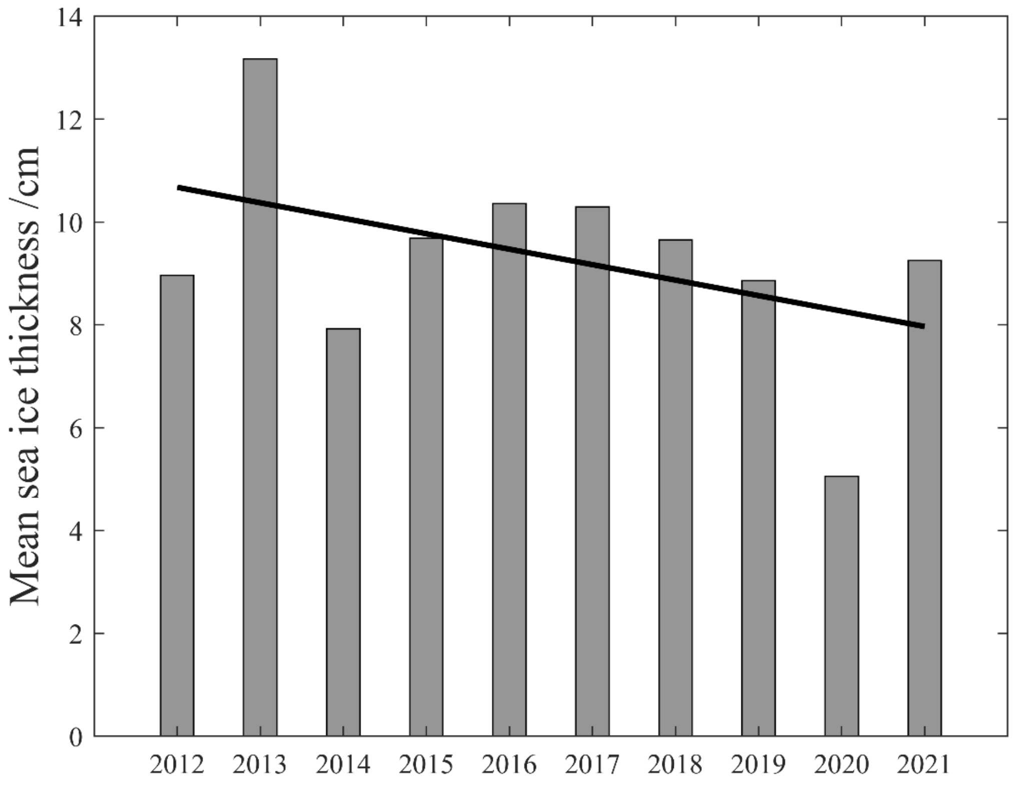

Annual **maximum** sea ice thickness

-0.56 cm/year

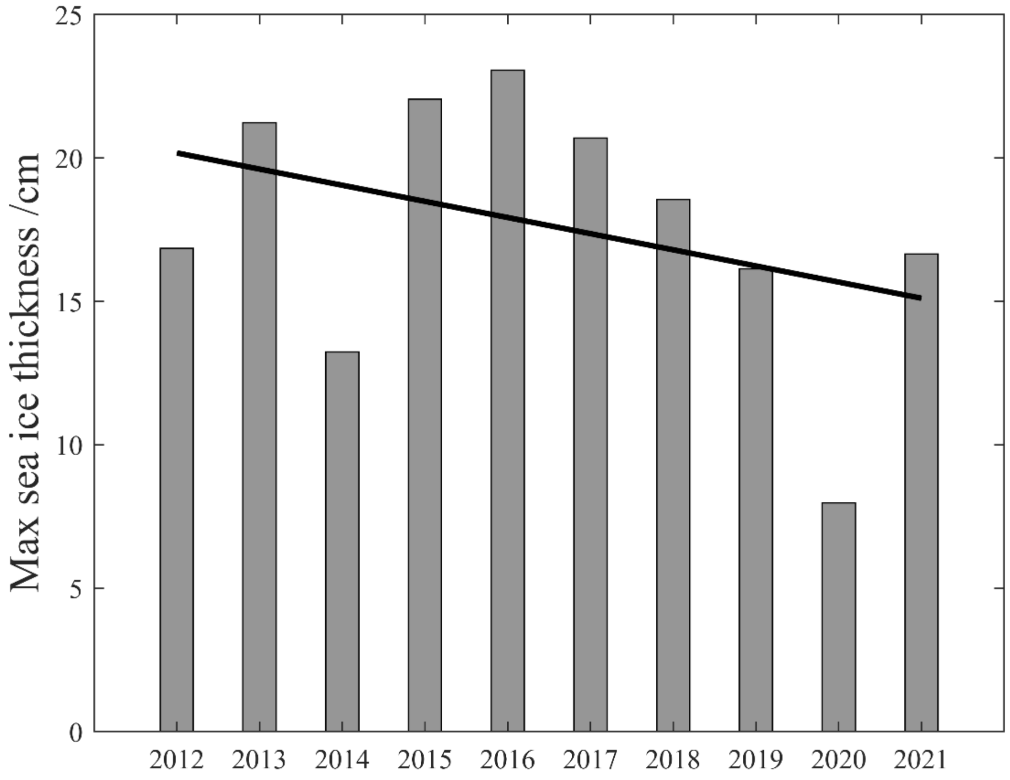

Decadal changes of sea ice drift

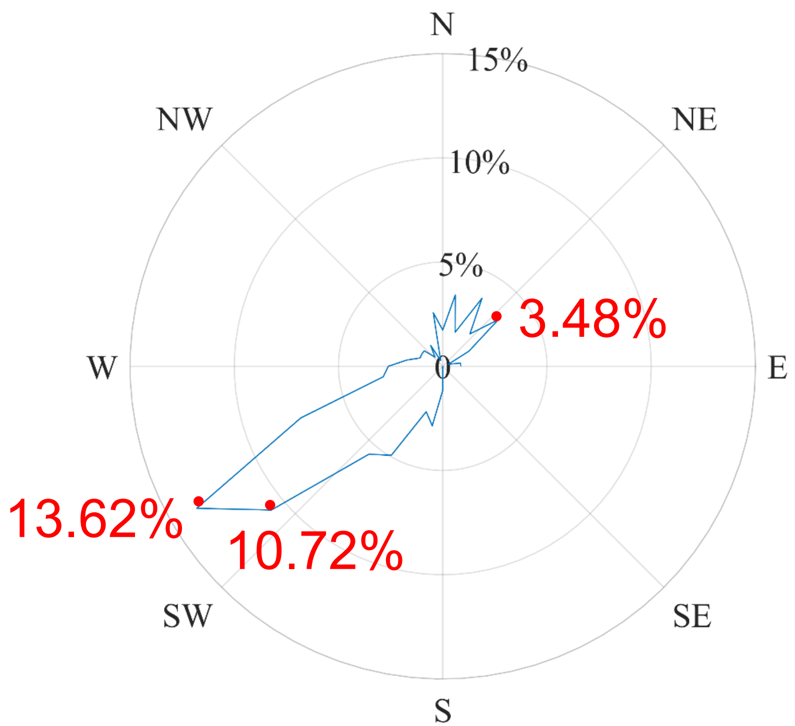

The frequency of sea ice drift direction

- SW, largest proportion;
- NE, small proportion;
- NW and SE: little proportion;

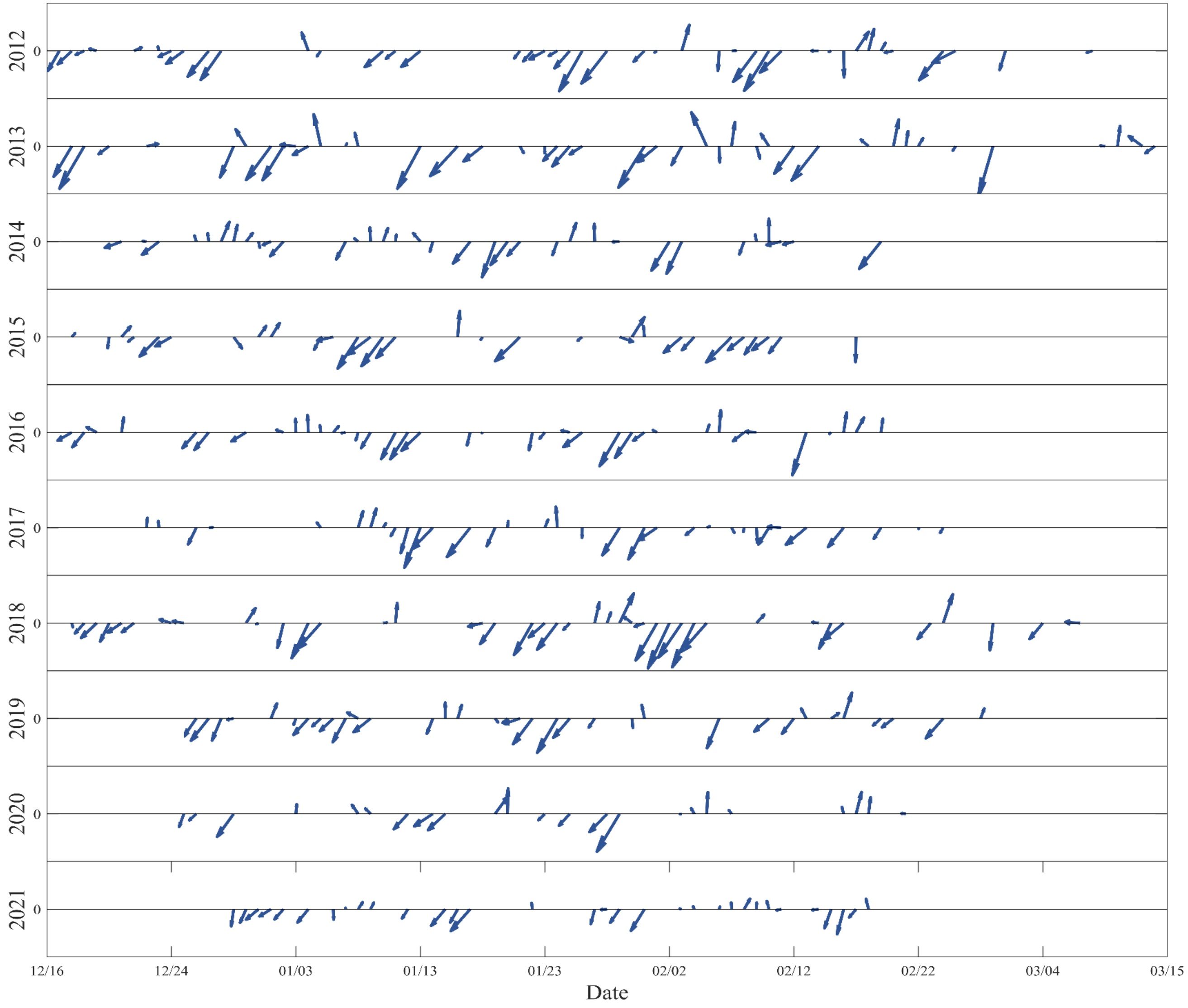

The interannual characteristics is not obvious.

Sea ice prediction models based on decadal statistics

- Cumulative negative temperature is key to predict the change of sea ice.
- We analyze the correlation between cumulative negative air temperature-Days with ice area and ice thickness.

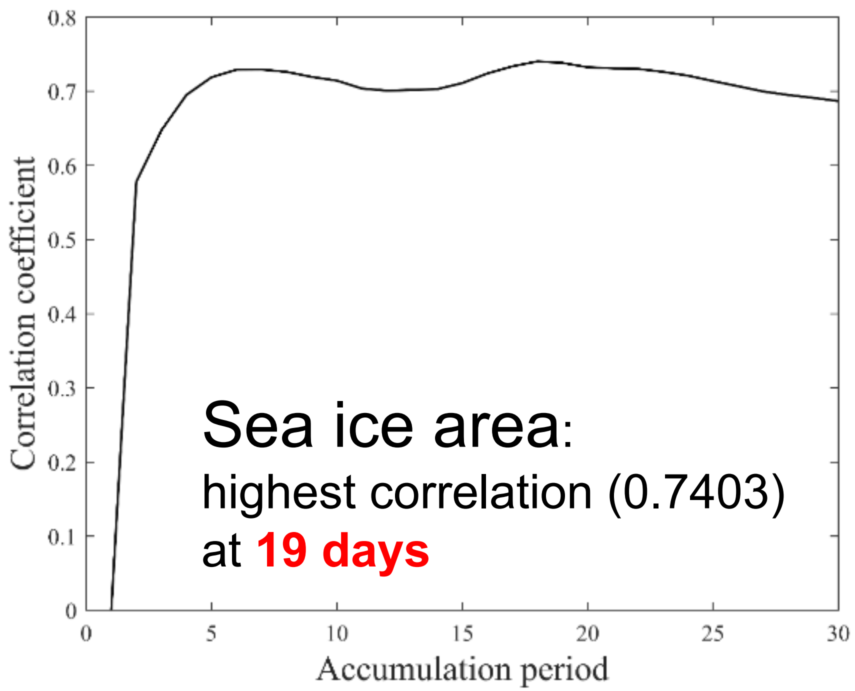

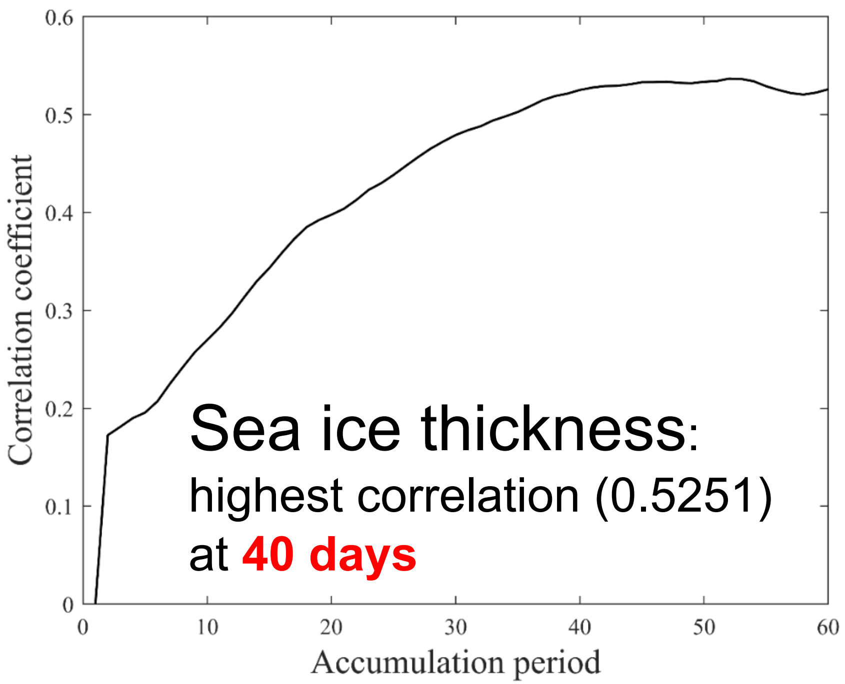

Sea ice area prediction model

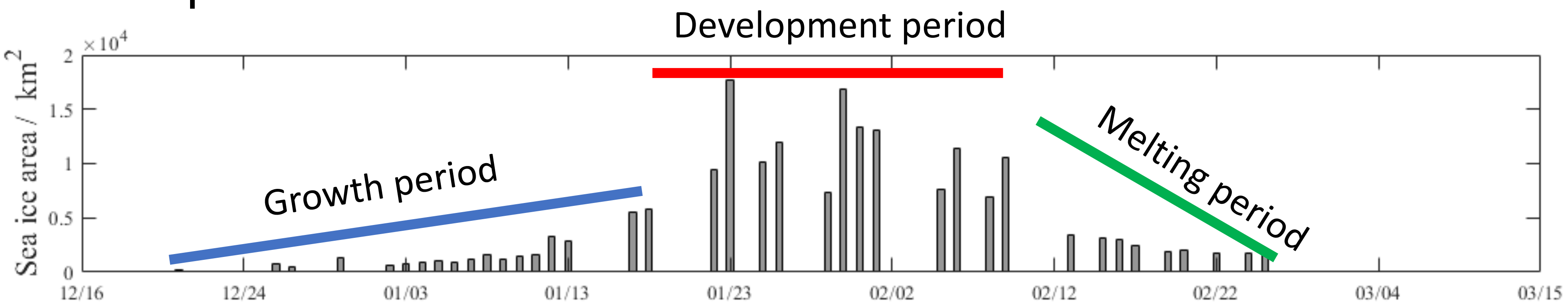

Growth period

$$S = -28.19t_{AT} - 51.35v_{wind} + 305.93$$

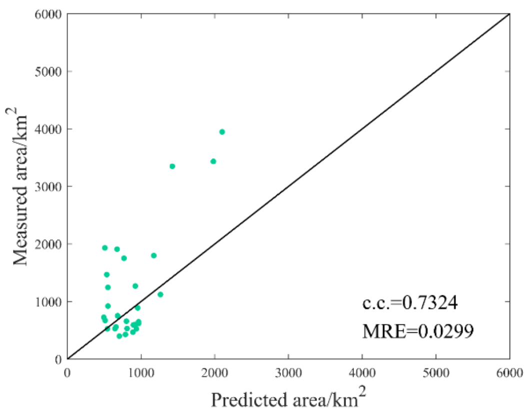

Development period

$$S = -91.99t_{AT} - 90.82v_{wind} + 773.49$$

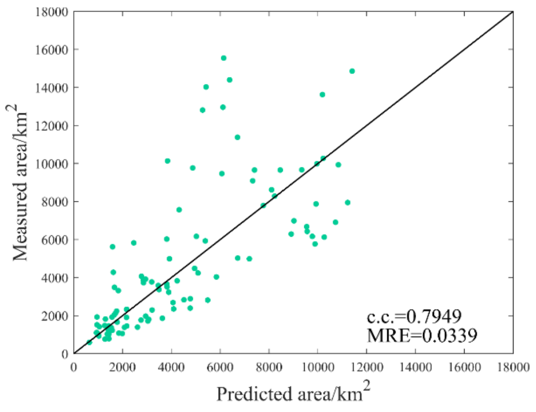

Melting period

$$S = -107.65t_{AT} + 251.71v_{wind} - 393.92$$

$$S = 4.07\times10^{-8}\times e^{-0.44t_{AT}} - 45v_{wind} + 1685.1$$

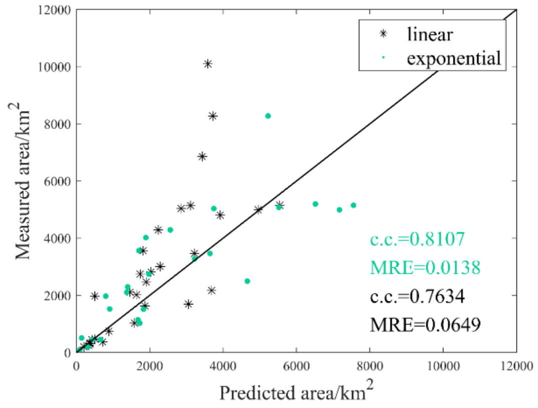

All periods

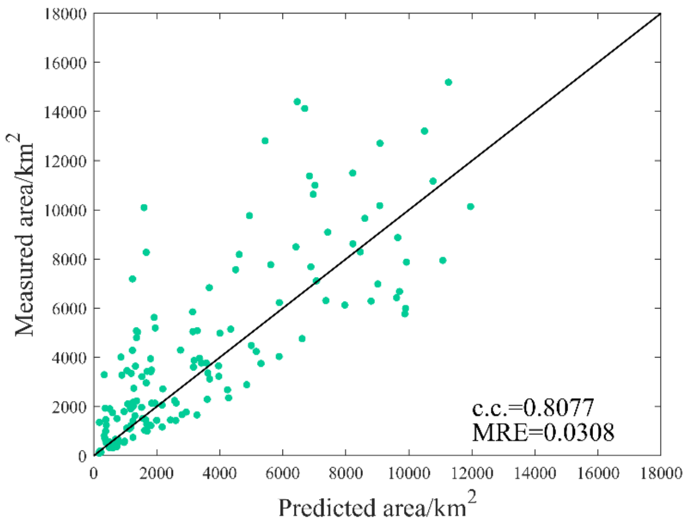

Sea ice thick prediction model

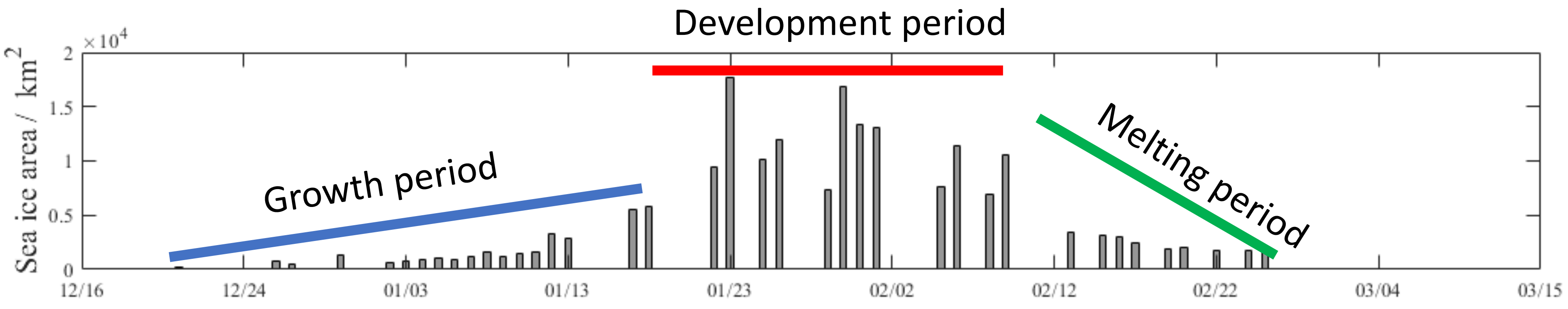

Growth period

$$H = -0.017t_{AT} - 0.29v_{wind} + 0.56$$

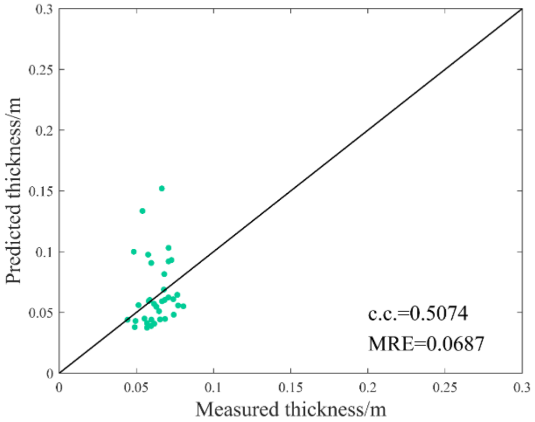

Development period

$$H = -0.041t_{AT} - 0.1v_{wind} + 8.38$$

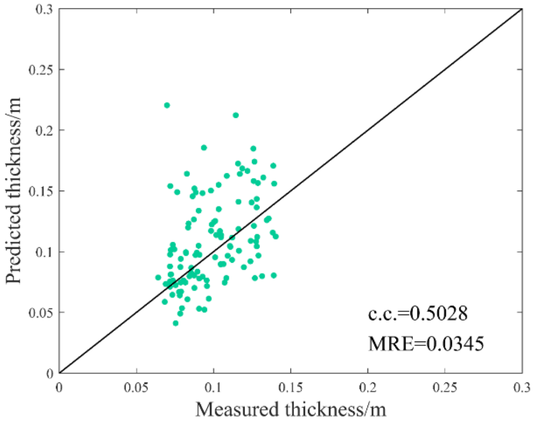

Melting period

$$H = -0.048t_{AT} - 0.26v_{wind} + 0.76$$

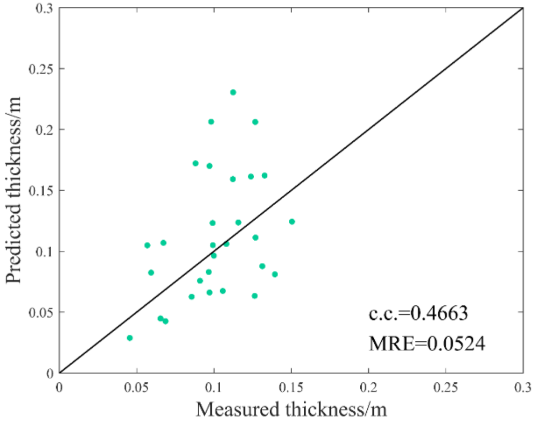

All periods

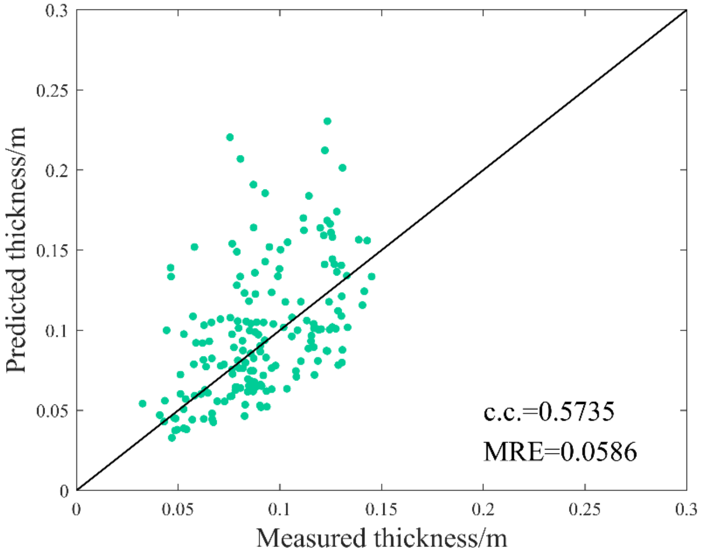

Sea ice drift prediction model (Neglecting the influence of internal ice stresses)

$$\vec{v}_{ice} = a\vec{v}_{wind} + b\vec{v}_{cur}$$

a — drag coefficients of wind

b — drag coefficients of current

$$\begin{bmatrix} v_{ice_x} \\ v_{ice_y} \end{bmatrix} = \begin{bmatrix} a_1 & a_2 \\ a_3 & a_4 \end{bmatrix} \begin{bmatrix} v_{wind_x} \\ v_{wind_y} \end{bmatrix} + \begin{bmatrix} b_1 & b_2 \\ b_3 & b_4 \end{bmatrix} \begin{bmatrix} v_{cur_x} \\ v_{cur_y} \end{bmatrix}$$

$$a = \begin{bmatrix} 0.0196 & -0.0555 \\ -0.0144 & -0.0089 \end{bmatrix}$$

$$b = \begin{bmatrix} -1.1380 & 4.9278 \\ 0.6052 & 2.2060 \end{bmatrix}$$

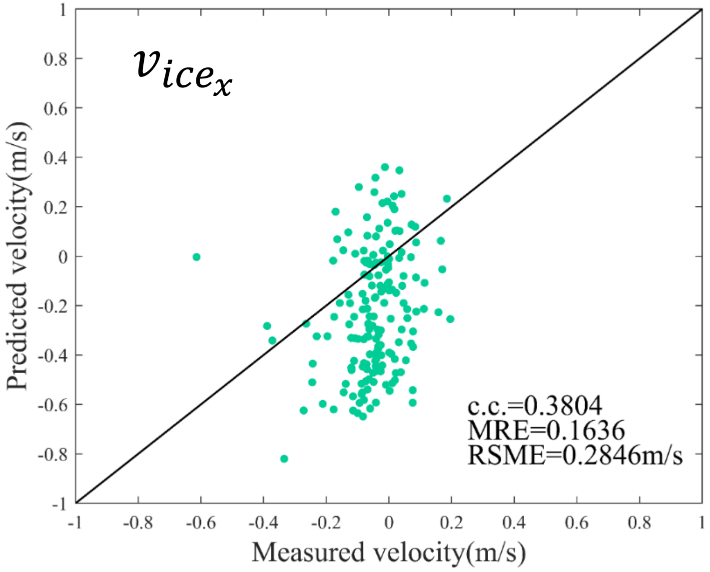

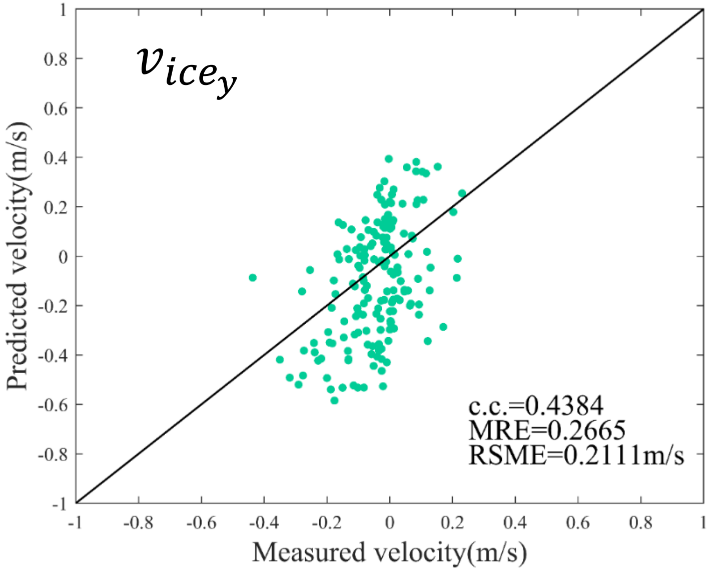

Reasons for error:

- The model is simple and needs to be improved
- Wind and current data are from ECMWF ERA5

EO Data Delivery

Data access (list all missions and issues if any). NB. in the tables please insert cumulative figures (since July 2020) for no. of scenes of high bit rate data (e.g. S1 100 scenes). If data delivery is low bit rate by ftp, insert “ftp”

ESA Third Party Missions	No. Scenes
1. ALOS PALSAR	6
2. RadarSAT-2	16
3. Cosmo-SkyMed	6
4.	
5.	
6.	
Total:	

Issues:
Iceberg detection, University in Tromsø/Norway: ESA-Agreement with JAXA: PALSAR-2 FB and WB images since April 2019 (not specifically via Dragon)

ESA Third Party Missions	No. Scenes
1. Sentinel-1	45
2. Sentinel-3 SLAT	2017~2023
3. CryoSat-2	2017~2023
4.	
5.	
6.	
Total:	

Issues:
Iceberg detection, University in Tromsø/Norway: S1 and S2 images via Science Hub since April 2019 (not specifically via Dragon)

Chinese EO data	No. Scenes
1. HY-2B	2018~2023
2. GF-3	45
3. FY-3C	2019~2023
4.	
5.	
6.	
Total:	

Issues:

III. Cooperation

- FIO, AWI, FMI, and NSOAS continue to develop sea ice thickness retrieval algorithms.
- NSOAS, FMI and DMI develop sea ice concentration estimation and SIC noise reduction algorithms.
- Joint effort by AWI/UiT, FIO, FMI, and SCMU is in preparation to deal with the detection of icebergs in sea ice.
- Cooperations with ice services world-wide (e.g. Denmark, Norway, Sweden, Canada, US, Argentina), plus Chalmers Technical University in Gothenburg, Sweden.
- The work of sea ice thickness detection work was selected for China-EU Space Science and Technology Cooperation Briefing.

International Glaciological Society

Arctic thin ice detection using AMSR2 and FY-3C MWRI radiometer data

Marko Mäkynen[1], Lijian Shi[2], and Xi Zhang[3]

1) Finnish Meteorological Institute

2) National Satellite Ocean Application Service, Ministry of Natural Resources, China

3) First Institute of Oceanography, Ministry of Natural Resources, Qingdao, China

ILMATIETEEN LAITOS
METEOROLOGISKA INSTITUTET
FINNISH METEOROLOGICAL INSTITUTE

IV. Young scientists and Publications

Name	Institution	Poster title	Contribution
Laust Færch	UiT The Arctic University of Norway	Variations of Signature Contrast Between Icebergs and Sea Ice Dependent on Ice Conditions and Radar Parameters	Iceberg
Xiao-yi Shen	Nanjing University	An Observation of Arctic Melt Ponds Based on Sentinel-2 and ICESat-2	Melt ponds
Wen-shuo Zhu	Shandong University of Science and Technology	Comparison of Doppler-Derived Sea Ice Radial Surface Velocity Measurement Methods from Sentinel-1A IW data	Sea ice drift
Jun-hui Zhu	Shandong University of Science and Technology	Enhanced-resolution reconstruction for the China-France Oceanography Satellite scatterometer	Sea ice drift
Ran Yan	Qingdao University	Sea Ice Parameter Retrieval In The Bohai Sea Using GOCI Data From 2011-2020	Ice concentration, thickness, drift
Wen-long Bi	Qingdao University	Inversion Of Sea Ice Concentration And Thickness In The Yellow Sea And Bohai Sea Based On HY-1C Data	Ice concentration, thickness

① Sun X, Zhang Xi, Huang W, et al. Sea Ice Classification Using Mutually Guided Contexts. IEEE Transactions on Geoscience and Remote Sensing, 2023.

② Dierking W., Zhang X., and co-authors, “Using New Ocean Remote Sensing Data for Operational Applications: Results from the Dragon 4 Cooperation Project”, Remote Sensing, 2021, 13, 2847.

③ Dierking W. et al., “Synergistic used of L- and C-band SAR satellites for sea ice monitoring”, IGARSS 2021.

④ Zhang X. et al., “Arctic Sea Ice Classification Based on HY-2B Dual-band Radar Altimeter Data during Winter to Early Spring Conditions”, IEEE JSTARS, 2021, 14: 9855-9872.

⑤ Shi L., et al., Sea Ice Concentration Products over Polar Regions with Chinese FY3C/MWRI Data. Remote Sens. 2021, 13, 2174.

⑥ Dong Z, Shi L, Lin M, et al. Feasibility of retrieving Arctic sea ice thickness from the Chinese HY-2B Ku-band radar altimeter. The Cryosphere, 2023, 17(3): 1389-1410.

⑦ Dong Z. et al., A Suitable Retrieval Algorithm of Arctic Snow Depths with AMSR-2 and Its Application to Sea Ice Thicknesses of Cryosat-2 Data. Remote Sensing, 2022, 14, 1041.

⑧ Wu S, Shi L, Zou B, et al. Daily Sea Ice Concentration Product over Polar Regions Based on Brightness Temperature Data from the HY-2B SMR Sensor. Remote Sensing, 2023, 15(6): 1692.

⑨ Liu M., et al. "Arctic Sea Ice Classification Based on CFOSAT SWIM Data at Multiple Small Incidence Angles." Remote Sensing, 2021, 14, 91.

⑩ Liu M., et al. "Sea ice recognition for CFOSAT SWIM at multiple small incidence angles in the Arctic." Front. Mar. Sci., 2022, 9: 986228.

⑪ Fang H., Zhang X., et al. Evaluation of Arctic Sea Ice Drift Products based on FY-3, HY-2, AMSR2 and SSMIS Radiometer Data. Remote Sensing. 2022, 14(20), 5161.

⑫ Wang R, Zhu J, Zhang X, et al. Enhanced-resolution reconstruction for the China-France Oceanography Satellite scatterometer. Geocarto International, 2023, 38(1): 2189315.

⑬ Wang R, Zhu W, Zhang X, et al. Comparison of Doppler-Derived Sea Ice Radial Surface Velocity Measurement Methods From Sentinel-1A IW Data. IEEE JSTARS, 2023, 16: 2178-2191.

⑭ Xiaoyi Shen et al. Snow depth product over Antarctic sea ice from 2002 to 2020 using multisource passive microwave radiometers. Earth System Science Data, 2022, 14(2): 619-636.

⑮ Xiaoyi Shen et al. Assessment of Arctic sea ice thickness estimates from ICESat-2 using IceBird airborne measurements. IEEE Transactions on Geoscience and Remote Sensing, 2021, 59(5): 3764-3775.

⑯ Xiaoyi Shen et al. Thinner Sea Ice Contribution to the Remarkable Polynya Formation North of Greenland in August 2018. Advances in Atmospheric Sciences, 2021, 38(9): 1474-1485.

V. Next planning

- Iceberg detection: improvement of algorithms, comparison and selection of optimal one(s), collection of data for validation, validation, building semi-operational environment (the key work of Sino-European joint effort).
- Sea ice drift: develop algorithm for Chinese HY-2 radiometer and for alignment of C- and L-band images (at AWI and University in Tromsø)
- Sea ice thickness: Altimeter + SAR to improve the spatial resolution of sea ice thickness product.

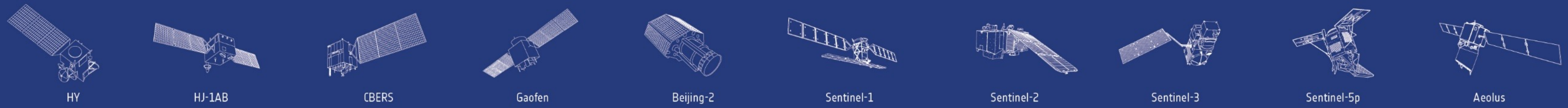
HY
HJ-1AB
CBERS
Gaofen
Beijing-2
Sentinel-1
Sentinel-2
Sentinel-3
Sentinel-5p
Aeolus

Thank you !